

Synergistic Correlates of Self-Dissolution in Meditation: Global Increases and Selective Reductions in Neural Complexity

Daniel A. Atad^{*1,2,3}, Pedro A. Mediano^{4,5}, Fynn-Mathis Trautwein⁶, Yair Dor-Ziderman^{1,2,3}, Henrik Rohr^{6,7} Yoav Schweitzer^{2,3}, Ohad Nave⁸, Stephen Fulder⁹, Aviva Berkovich-Ohana^{1,2,3}

1. School of Therapy, Counseling and Human Development, Faculty of Education, University of Haifa, Haifa 3103301, Israel
2. The Integrated Brain and Behavior Research Center (IBBRC), University of Haifa, Haifa 3103301, Israel
3. Edmond Safra Brain Research Center, Faculty of Education, University of Haifa, Haifa 3103301, Israel
4. Department of Computing, Imperial College London, 180 Queen's Gate, South Kensington, London SW7 2RH, United Kingdom
5. Division of Psychology and Language Sciences, University College London, 26 Bedford Way, London WC1H 0AP, United Kingdom
6. Department of Psychosomatic Medicine and Psychotherapy, Medical Center - University of Freiburg, Faculty of Medicine, University of Freiburg, Freiburg im Breisgau 79104, Germany
7. Bernoulli Institute for Mathematics, Computer Science and Artificial Intelligence, University of Groningen, Netherlands
8. Department of Cognitive Sciences, Hebrew University of Jerusalem, Jerusalem 9190501, Israel
9. The Israel Insight Society (Tovana), Kibbutz Ein-Dor, R.D. Izrael 1933500, Israel

* Corresponding Author: danielatad@gmail.com

Author Contributions:

DAA: MEG data analysis, manuscript writing; PAM: MEG data analysis, supervision, manuscript revision; FMT: MEG data analysis, manuscript revision; YDZ: MEG data cleaning, manuscript revision; HR: MEG data analysis; YS: MEG data collection, data cleaning; ON: phenomenological interviews and analysis; SF: meditation instructions and support of data collection; ABO: supervision, manuscript revision.

Funding:

This work was supported by the Tiny Blue Dot Foundation Grant Number TBD-43777846, Israel Scientific Foundation (ISF) Grant Number 677/21.

Conflicts of Interest:

The authors declare no competing financial interests

Abstract

A fundamental aspect of human experience is that of being a bounded and embodied agent. This basic sense of self typically operates implicitly, yet traditional contemplative accounts alongside recent work in philosophy, phenomenology and neuroscience suggests that it can be attenuated or even fully dissolved while retaining awareness. Here we present an extended analysis of data from a large-scale neurophenomenological study investigating such minimal modes of awareness, in which 46 long-term meditators alternated between resting-state and meditative conditions of self-boundary (SB) dissolution and maintenance during magnetoencephalography. Results show global increases in broadband entropy rate and directed information transfer in both meditation conditions compared to rest. Spectral decomposition of both measures reveals that broadband effects are driven mostly by high-frequency activity, and that information transfer and entropy rates exhibit qualitatively different spectral patterns. Although these global changes don't clearly differentiate meditative self-boundary dissolution, localized reductions in information transfer from the anterior cingulate to mid and post cingulate and in high-beta entropy rate in sensorimotor and posterior-medial cortices did differentiate the meditation conditions. Furthermore, a relative reduction of broadband orbitofrontal cortex entropy rate, and broadband information transfer from occipital, cingulate, limbic and subcortical areas, both correlated strongly with SB-dissolution phenomenology. Together with a previously reported neural correlate from the same dataset of reduced high-beta power in the posterior-medial cortex, these two neural correlates synergistically explained over half the variance in phenomenological dissolution scores ($R^2 = 0.52$), exhibiting a neurophenomenological association of unprecedented strength. By integrating nuanced phenomenology with multiscale neural metrics, our findings provide novel insight into self-attenuation and advance the empirical investigation of minimal phenomenal experience.

1. Introduction

The sense of self is a core feature of ordinary conscious experience (Blanke, 2012; Christoff et al., 2011; Gallagher, 2000; James, 1890). Theoretical accounts describe the self as a dynamic construct or process with various aspects (Gallagher, 2013; Gallagher & Zahavi, 2005; Metzinger, 2003), yet many converge on a distinction between two main aspects - the reflective ("me") and pre-reflective ("I") sense of self (e.g. in Damasio, 1999; Gallagher, 2000; James, 1890). The latter, more basic form of self-consciousness has been referred to as minimal self (Gallagher, 2000), minimal phenomenal selfhood (Blanke & Metzinger, 2009), pre-reflective self (Legrand, 2006) and embodied self (Seth, 2013) and is thought to be the fundamental layer on which other aspects are built. This aspect of the self is typically manifested through features such as self-location, a first-person perspective, a sense of body ownership and a sense of agency – which together constitute a dynamic functional boundary between self and non-self (Christoff et al., 2011; Ratcliffe, 2008). While usually implicit and persisting, these features can undergo profound alteration, and attenuation, in altered states of consciousness such as meditative and psychedelic states (Josipovic, 2014; Letheby & Gerrans, 2017; Millière et al., 2018; Nave et al., 2021). Such attenuations in the sense of self are a hallmark of states described as "pure awareness" or "minimal phenomenal experience" (MPE) (Metzinger, 2020; Windt, 2015). These are thought of as the simplest form of detectable conscious experience, with minimal or

no conceptual content and devoid of representations of self, time and a spatial frame of reference (Metzinger, 2020). The occurrence of such states during meditation have been demonstrated and phenomenologically characterized in an initial yet comprehensive project (Gamma & Metzinger, 2021; Metzinger, 2024). MPEs have been suggested as a unique entry point to the study of consciousness, potentially allowing a minimal-model explanation for consciousness by accounting for the core causal factors giving rise to the phenomenon (Metzinger, 2020). Therefore, systematically studying states in which the sense of self, down to its most minimal and basic embodied aspects, are attenuated hold potential for advancing the scientific study of consciousness.

Given the implicit nature of the minimal self, operationalizing it for empirical research is inherently difficult. However, this difficulty can be addressed by leveraging two key elements: the trained skills of long-term meditation practitioners, and in-depth phenomenological interviews, which allow suspension of naive beliefs about one's experience and guide attention toward its pre-reflective facets (Petitmengin, 2006; Varela & Shear, 1999). Accumulating evidence suggests that long-term meditators can reliably and repeatedly enter targeted altered states of consciousness (Lutz et al., 2007, Thompson et al., 2005), and can suspend multiple facets of selfhood during global forms of self-dissolution (Ataria et al., 2015; Dor-Ziderman et al., 2013, 2016). The ability to volitionally enter such states renders long-term meditators as a uniquely fit population for neurophenomenological investigation dissolution of the minimal, pre-reflective self. Neurophenomenology (Varela, 1996) offers a framework for bridging the explanatory gap between first-person experience and third-person physiology by combining first-person methods such as phenomenological interviewing, with third-person physiological measures in an iterative cycle (Berkovich-Ohana et al., 2020). This approach has proven effective for systematically characterizing altered states of consciousness (reviewed in Timmerman et al., 2023).

Building on this promising methodological ground, in this paper we attempt a comprehensive exploratory analysis of a unique and large-scale neurophenomenological dataset investigating self-boundary (SB) dissolution in meditation (Nave et al., 2021; Trautwein et al., 2024). The data were obtained from 46 experienced meditators who entered meditative states in which they volitionally attenuated their self-boundaries, alongside an active-control meditative state of maintaining self-boundaries and a resting state (see Methods for elaboration). Interviews inspired by the micro-phenomenological method (Petitmengin, 2006) were conducted, participants' experiences were mapped and the success of SB-dissolution was subsequently quantified (Nave et al., 2021). Participants that achieved full-fledged SB-dissolution reported an immersion in undifferentiated space, lacking first-person observer position and distinctions between experienced content and experiencing subject (Nave et al., 2021). Although such states usually retain some residual experiential qualities, they approach MPE by minimizing distinguishable conceptual and structural representations of self and world. MPE have been described through qualitative and quantitative retrospective reports (Gamma & Metzinger, 2021), yet reproductions in the lab as well as close-up microphenomenology is still lacking (but see Alcaraz-Sanchez, 2023). From this perspective, the present dataset presents an unprecedented opportunity to investigate one potential candidate of MPE-like states as realized in deconstructive meditative practices (Dahl et al., 2015). Importantly, this dataset holds several unique advantages. First, in-depth phenomenology was systematically captured and clustered into dimensions that could be quantified across individuals. This combination of qualitative depth and quantitative structure provides an unusually rich account of altered self-experience. Second, the contrast to an active-control meditative state identification of specific phenomenological features and neural dynamics that are unique to SB-dissolution beyond global effects of meditation. Third, both the usage of active-control SB maintenance and the varying degrees

of success in SB-dissolution achieved by participants, allow us to approximate a trajectory of phenomenal and neural processes towards full-fledged SB-dissolution.

Previous confirmatory analysis of our neurophenomenological MEG dataset has linked the suspension of the minimal self to reduction in high-beta power in the posterior-medial cortex, and most prominently at the peak frequency of 27 Hz in bilateral posterior cingulate and precuneus areas (Trautwein et al., 2024). These results replicated findings from proof-of-concept study and a case study informing it (Dor-Ziderman et al., 2013; 2016, respectively) and provided robust evidence supporting both the feasibility of studying such deep meditative states through neurophenomenology. However, spectral power alone lacks explanatory power for a mechanistic interpretation of such states that aims to relate neural dynamics to computational models. Therefore, here we present an extended analysis of the same neurophenomenological MEG dataset that includes various complexity measures. The use of measures inspired by complexity science and information theory in neuroscience has been gaining increasing traction in recent years, and converging evidence suggests an opportunity for characterizing global states of consciousness beyond traditional approaches (Sarasso et al., 2021). Our analyses focus on complementary metrics for assessing the complexity of neural activity. Lempel–Ziv complexity (LZc; Lempel & Ziv, 1976) and Complexity via State-Space Entropy Rate (CSER; Mediano et al., 2023) both estimate the entropy rate of neural activity within single regions, while Transfer Entropy (TE; Schreiber, 2000; Bossomaier et al., 2016) estimates directed information transfer between regions. LZc and CSER can be taken as proxies for the differentiation of neural activity, and TE as a proxy for integration (Mediano et al., 2022; Sarasso et al., 2021). Integration and differentiation of neural activity are important organizing principles in the neuroscience of consciousness (Tononi et al., 2016; Tononi & Edelman, 1998), and a systematic exploration of the balance between them in various altered states, and specifically in MPE-like states holds promise for advancing our understanding of consciousness (Mediano et al., 2022). A growing body of research suggests that in meditative states entropy tends to increase globally compared to rest (recently reviewed by Atad et al., 2025), yet most studies lack nuance that could be derived from a spectral decomposition of entropy rate as possible in CSER, and from source-localized MEG data. Furthermore, to the best of our knowledge, directed information transfer has received very limited attention in meditation studies, therefore the application of TE here introduces a novelty in the field. Finally, the use of complexity measures, as applied here, hold potential for validating predictions of novel formal computational phenomenology models, which attempt to draw mechanistic links between phenomenology and physiological measurements (Lutz et al., 2025; Ramstead et al., 2022).

In sum, we address two main questions in the current analysis: How meditative states affect neural information dynamics, and whether self-dissolution phenomenology can be explained by such metrics.

2. Materials and Methods

We re-analyzed a neuro-phenomenological dataset consisting of magnetoencephalography (MEG) recordings and phenomenological interviews previously collected in our lab. In section 2.1 we briefly describe the experimental setup, data collection and cleaning conducted in the previous study, for a full description see Nave et al. (2021) and Trautwein et al. (2024). In sections 2.2-2.4 we describe the methods applied in the current study.

2.1 Data Acquisition

Participants: N=46 meditation practitioners (aged 26–72, mean age = 39.8 ± 10.9 , 27 males and 19 females) with a wide range of meditation experience (115–24,837 hours, mean = $3,832 \pm 4,845$ hours) in mindful awareness and insight (vipassana) practice. Participants were selected to represent a wide variety in expertise levels to allow the detection of expertise-dependent effects. Inclusion criteria were the attendance of at least one meditation retreat and a minimum of one year of practice. Exclusion criteria were current psychiatric disorders or medication, conditions that limit MEG data quality, and not having normal or corrected-to-normal vision or hearing. During preprocessing of the MEG data, one participant was excluded due to large artifacts, resulting in a sample size of N=45. All participants had participated in a preparatory 3-week meditation training program designed to explore more directly the sense of self-boundary and its dissolution.

MEG recordings: Conducted in the supine position using a whole-head 248-channel magnetometer array (4-D Neuroimaging, Magnes 3600 WH) with a sampling rate of 1017.25 Hz and an online 1–400 Hz band-pass filter in a magnetically-shielded room. Environmental noise was removed by reference coils, and head shape and coil position were digitized. MEG data cleaning involved removal of artifacts caused by heartbeats (corrected via electrocardiogram estimate based on the MEG average), power line frequency (corrected via recording on an extra channel) and building vibrations (corrected via recordings from accelerometers on the MEG gantry). Furthermore, two sensors showed excessive noise across recording sessions and were therefore removed from all recordings. Movement and jump artifacts were removed by visual inspection and Independent Component Analysis.

Experimental procedure: During MEG acquisition, participants were asked to alternate between a non-meditative resting state in which they let their minds wander freely, a state of self-boundary dissolution (SB-) in which they were asked to meditate while dissolving their sense of self-boundary, and a state of self-boundary maintenance (SB+) in which they were asked to meditate while maintaining a clear sense of their self boundaries. The procedure involved two experimental blocks (Fig. 1B) which included a 100-seconds resting state followed by 5 repetitions of 60-seconds meditation epochs, alternating between meditative states of SB+ or SB-. The order of SB+ and SB- was counterbalanced, so that half of the participants started with SB+ in the first block and with SB- in the second block and vice versa for the second half of the cohort. After each block participants were asked to rate the depth and stability of each meditative epoch (on a scale of 1–3). Following the two blocks, an additional 100-seconds resting state was recorded. Self-ratings indicated that, overall, participants felt successful in dissolving and maintaining the SB during MEG assessments (Fig. 1B, for an analysis of depth and stability ratings see Trautwein et al., 2024). Together with the phenomenological data, these results confirm, on an experiential level, the successful induction of meditation-based SB-dissolution in the lab, subsuming several core features of the minimal self.

Phenomenological interviews and analysis: directly after the MEG session, semi-structured interviews inspired by the micro-phenomenological method (Petitmengin, 2006) were conducted to describe the actual experience of meditation-based self-boundary dissolution (SB-) and maintenance (SB+). Based on the interviews, six phenomenological dimensions were derived - sense of agency, self-location, first-person perspective (FPP), attentional disposition, body sensations and affective valence with three to four subcategories for each dimension (see Nave et al., 2021). Two independent raters coded each dimension, and a quantitative depth of dissolution score (Dissolution Depth Calculated, DDC) was derived for each participant based on the semantic order of the subcategories and their cross-correlation. Specifically, DDC was defined as the weighted sum of all the phenomenological

dimensions excluding affective valence (see Trautwein et al., 2024). Furthermore, scores on three dimensions corresponding to core facets of the minimal self—agency, FPP, and self-location (Blanke and Metzinger, 2009)—were used to select a subgroup of “full dissolvers” ($N = 12$) that included only participants having the highest rating on at least one dimension and the second highest rating on the remaining dimensions during self-boundary dissolution (SB-) state (Fig. 1A). For contrasts involving the self-boundary maintenance (SB+) condition, one participant who reported characteristics of a dissolution state also in the maintenance condition was excluded from the analysis (see Trautwein et al., 2024).

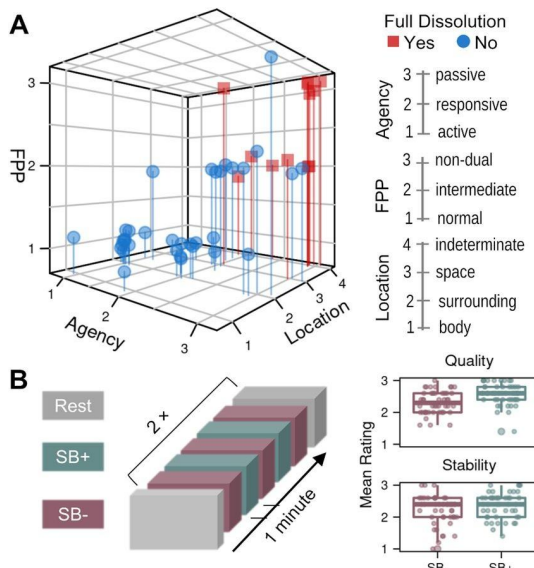


Figure 1. Study design and phenomenology-derived subgroups.

A: Phenomenological space spanned by three dimensions demarcating core facets of the minimal self. Participants were mapped onto these dimensions based on phenomenological interviews (for details on the dimensions, see Nave et al. 2021). **B:** Representation of the sequence of rest and meditation states during MEG assessment (SB+, self-boundary maintenance; SB-, to self-boundary dissolution). Boxplots show mean values of self-reported quality and stability of the meditation, rated after each state. Adapted with permission from Trautwein et al., 2024.

2.2 Data Preprocessing and Source Reconstruction

For each participant, a semi-realistic head model of volume conduction (Nolte, 2003) was constructed based on a single-subject MRI template that was linearly mapped to fit each participant's digitized head shape. A regular three-dimensional source grid (1 cm resolution) was inversely warped to fit the participant's head model. For each grid position, a lead field matrix was computed according to the head position in the MEG system and the volume conduction model. Sources were localized using a linearly constrained minimum-variance (LCMV) beamformer (Van Veen et al., 1997) as implemented in Fieldtrip software (Oostenveld et al. 2011). The LCMV beamformer yielded a spatial filter (covariance) matrix derived from the sensor data of the entire recording. The spatial filter was then multiplied by sensor activity to yield 1457 “virtual electrodes” (Hillebrand et al., 2005), each including the estimated neural activity time-series at each predefined source location (“voxel”). Virtual electrode data was downsampled by a factor of 5 to a sampling frequency of ~200 Hz and band-pass filtered at 1–100 Hz using the default settings in Fieldtrip software of a two-pass 4th-order Butterworth filter. For transfer entropy analyses we parcelated the voxel-level data using the Automated Anatomical Labeling 116 (AAL-116) atlas, an extended version of the original AAL atlas (Tzourio-Mazoyer et al., 2002).

2.3 Measures of Neural Complexity

All measures in the following analysis were computed on 6-second time windows and then averaged per experimental condition (see details below). Code for all neural complexity measures is available at <https://github.com/pmediano/EntRate>.

2.3.1 Lempel-Ziv complexity

Lempel-Ziv complexity (LZc) is a measure of the diversity of patterns in a discrete sequence. Theoretically, in the limit of an infinitely long binary sequence, LZc converges to the entropy rate of the process generating the sequence, provided the process is ergodic (Lempel & Ziv, 1976; Ziv, 1978). In neuroscience, entropy rate estimators such as LZc are widely applied and robustly validated measures of neural dynamics that can differentiate global states of consciousness (Sarasso et al., 2021). Typically, when compared to waking rest, lower LZc of neuroimaging data has been associated with states of reduced levels or absent conscious awareness such as deep sleep (Aamodt et al., 2023) or anaesthesia (Schartner et al., 2015; Zhang et al., 2001), while LZc is typically higher in altered states of consciousness such as psychedelic intake (Mediano et al., 2024; Schartner et al., 2017; Timmermann et al., 2019) and meditative states (D'Andrea et al., 2024; Lu & Rodriguez-Larios, 2022; Walter & Hinterberger, 2022; reviewed in Atad et al., 2025).

To calculate LZc, voxel-level data within each 6-second epoch was detrended and binarized using the mean of all samples in each epoch as a threshold, resulting in binary vectors of length $T \approx 1200$ data points, which suffices for the estimation of entropy rate via LZc (Amigó et al., 2004). For each binary vector, LZc was computed using the LZ76 algorithm (Kaspar & Schuster, 1987; Lempel & Ziv, 1976), which counts the number of distinct substrings in the binary vector. LZc is thus minimal if the vector only repeats the same value, and increases with a more diverse vector. The resulting LZc values were normalized by multiplying the computed value with $\frac{\log_2 T}{T}$. This normalisation ensures that a fully predictable signal is assigned a complexity value of 0, and a fully random (i.e. unpredictable) signal is assigned a value of 1. Unlike the other calculated measures (subsequently elaborated), LZc was calculated only for broadband activity (1-100 Hz), as calculating LZc on narrow-band signals can introduce various distortions stemming from the band-pass filtering of the signal (Mediano et al., 2023).

2.3.2 Complexity via State-Space Entropy Rate

Complexity via State-Space Entropy Rate (CSER, Mediano et al., 2023) is a recently developed complexity measure grounded in information theory, offering a principled estimator of the entropy rate of continuous neural signals without requiring discretization. CSER enables exact analytical spectral decomposition of the entropy rate into frequency components, thus allowing an estimation of neural complexity within frequency bands in a manner that does not suffer the distortions introduced when attempting such a calculation using LZc (Atad et al., 2025). This approach holds potential for gaining a more refined understanding of the neural dynamics contributing to overall complexity. The use of both measures in the current analysis allows us to be aligned with studies using the more common LZc while capitalizing on the advantages of CSER to provide a more nuanced analysis of entropy rate. As a relatively new measure, CSER has not yet been widely validated, but initial evidence demonstrates that indeed broadband CSER mirrors well-established effects seen in broadband LZc for various conscious states, while spectrally decomposed CSER shows more nuanced results for different frequency bands. Neural dynamics under various psychedelic substances exhibit an increase in broadband CSER and both increases and decreases in CSER for different frequency bands (Agnorelli et al., 2025; Mediano et al., 2023; Nikolic et al., 2024), and CSER is decreased in NREM sleep and anaesthesia compared to wakefulness (Mediano et al., 2023).

CSER models neural time-series as observations of an underlying hidden stochastic process using linear state-space models with Gaussian innovations. The entropy rate is then estimated from the residual variance of the model's one-step-ahead predictions—i.e., the variance (or covariance, in the multivariate case) of the prediction errors, also known as innovations. Under the assumption of Gaussian innovations, the CSER estimate of entropy rate can be computed directly using the standard formula for the differential entropy of a multivariate Gaussian distribution (see Mediano et al., 2023 for a full description). To calculate the spectrally decomposed entropy rate, CSER builds on an established theorem relating the residual variance and the spectral density of a stationary process (Hannan and Deistler, 2012, Th. 1.3.2), thus obtaining a principled expression for spectrally-decomposed entropy rate.

To calculate CSER, voxel-level data within each 6-second epoch was normalized to unit variance (z-scored). We calculated CSER both for broad-band (1–100 Hz) activity and for each canonical frequency band separately (see Supplementary Table 1 for frequency band definition). CSER thus complements LZc by offering a continuous, spectrally resolved perspective on neural complexity that supports finer-grained analysis of state- and task-dependent neural dynamics.

2.3.3 Transfer Entropy

Transfer Entropy (TE, Bossomaier et al., 2016; Schreiber, 2000) is an information-theoretic extension of Granger Causality (Barnett et al., 2009), which quantifies the degree of uncertainty reduced in predicting the next step in a time-series of target activity, when the activity of a source time-series is known. When applied to neuroimaging data, TE can be used to assess the dynamic interdependencies between the time-series generated by source and target regions in the brain, thus serving as a measure of directed functional connectivity, also termed effective connectivity (Vicente et al., 2011). TE is also a widely used and robustly validated measure of conscious states (e.g. Barnett et al., 2020; Rajpal et al., 2022), and serves in our analysis as a complementary measure to LZc and CSER, allowing an analysis of how different brain regions influence each other.

Mathematically, TE is defined as follows. Denote the activity of two given ROIs at time t by the vectors X_t and Y_t , and the activity of the rest of the brain by Z_t . TE is computed in terms of Shannon's mutual information, I , as the information about the future state of the target, Y_{t+1} , provided by X_t over and above the information in Y_t and Z_t :

$$TE Y \rightarrow X|Z = I(X_t; Y_{t+1}^- | X_{t-1}^-, Z_{t-1}^-)$$

Where X_{t-1}^- refers to the (possibly infinite) past of X_t up to and including time t (and analogously for Y_t and Z_t). This quantity is estimated using state-space models with Gaussian innovations (Barnett & Seth, 2015) and is calculated using an in-house script based on the MVGC toolbox (Barnett & Seth, 2014). Our in-house script allows both for a calculation of broad-band TE and of spectrally-decomposed TE, and thus we calculate TE for the broadband activity and per each canonical frequency band (see Supplementary Table 1). TE values were normalized by the mutual information between the past state of the whole brain and the future state of the target signal, $I(X_{t-1}^-, Y_{t-1}^-, Z_{t-1}^-; X_t)$, ensuring that TE is bounded between 0 and 1.

We calculate TE on AAL-116 parcellated time-series, using the 90 cortical and sub-cortical regions and excluding regions of the cerebellum, and. Following Barnett et al. (2020), we aggregate these into 8 regions of interest (ROIs) including the cingulate cortex, frontal lobe, limbic region, occipital lobe, parietal lobe, sensorimotor cortex, subcortical region, and temporal lobe (see Supplementary Table 2 for AAL-116 sources comprising each ROI). Note that here we refer to the average time-series obtained for each parcellation region as sources and to our aggregation of these sources as ROIs. We calculate TE both between and within ROIs as follows:

- Within ROI *pairwise-conditional* measures, which measure *univariate* TE between pairs of sources within each ROIs, conditioned on all other sources.
- Within ROI *global-conditional* measures, which measure the total statistical association of all sources within an ROI conditioned on all sources lying outside the ROI. For each target within the ROI we calculate the *multivariate* TE from all other sources within the ROI, and then averaging the TE values for all targets to get a single value per ROI.
- Between ROI *pairwise-conditional* measures, which measure *multivariate* TE between pairs of ROIs, conditioned on all other sources.

2.4 Statistical Analysis

Comparison between experimental conditions was carried out in a within-subjects design for the whole group (N=45), and a between-subjects design comparing the full dissolvers (N=12) and others (N=33) subgroups. In the comparisons including the SB+ condition, one subject from the full dissolvers group who reported characteristics of a dissolution state in this condition was additionally excluded from the analysis (see Trautwein et al., 2024 for details).

For LZc and CSER voxel-level data, whole-brain nonparametric cluster-based randomization tests, as implemented in FieldTrip (Maris and Oostenveld, 2007), were used to assess statistical significance. Specifically, clusters were formed by thresholding individual values at $p = 0.01$ (consistent with Trautwein et al., 2024) and then evaluated based on the maximum sum of t-values within a cluster. For the randomization distribution, 5000 permutations were drawn. Hypotheses were then evaluated at a two-tailed alpha threshold of $p = 0.05$.

For TE *pairwise-conditional* measures, statistical testing was carried out as in Rajpal et al. (2022). Namely, multiple comparisons were addressed using the Network-Based Statistic (NBS, Zalesky et al., 2010) method, which identifies clusters of differences while controlling for family-wise error rate. Our analysis used an in-house adapted version of NBS for directed networks, such as the ones resulting from TE analyses. The critical t-value for identifying clusters was set corresponding to $p < 0.05$, number of permutations was set to 5000 and hypotheses were evaluated at a two-tailed alpha threshold of $p = 0.05$. For TE *global-conditional* measures, each ROI had one value representing the average TE within it. Therefore, significance of differences between conditions was tested using a paired-samples t-test with a two-tailed alpha threshold of $p = 0.05$. To correct for multiple comparisons, p-values were adjusted using the false discovery rate method (FDR, Benjamini & Hochberg, 1995) procedure for two families of comparisons - within ROIs (8 ROIs and 3 condition comparisons - total of 24 tests), and significant differences were reported based on FDR-corrected q-values ($q < 0.05$).

Correlations with phenomenology were tested by taking the difference in neural measures between SB- and SB+ conditions as the dependent variable and the phenomenological dissolution score (DDC) as the independent variable. To preserve statistical power and avoid excessive post-hoc corrections for

multiple comparisons, correlations with DDC were restricted to broadband LZc voxel-level data and to broadband TE between ROIs, rather than within each ROI. Given that condition comparison results for LZc and CSER were highly similar, LZc was used as a representative measure for the correlation analysis (see Results). For LZc, correlation was tested via whole-brain nonparametric cluster-based randomization tests implemented using the FieldTrip ft_statfun_correlationT statistic, which computes voxel-wise Pearson correlations, and assesses cluster-level significance using the Monte Carlo method. For TE, our inhouse directed NBS method was used in the same manner as the condition comparisons, but with the design matrix including the DDC value. For both TE and LZc thresholds for identifying clusters and testing hypotheses were set as in the condition comparisons. After cluster and NBS correction, p-values of the correlations obtained from these tests were also FDR-corrected for multiple comparisons.

Finally, the values of the neural measures difference between SB- and SB+ for which there were significant correlations were included as predictors in a linear model predicting DDC, alongside pre-computed neural difference values of high-beta power in the posterior-medial cortex obtained from the previous analysis (See Trautwein et al., 2024, Fig. 3). Measures used in the linear model were z-scored in order to scale their absolute magnitude and allow for comparison of relative predictive power. Note that z-scoring the measures does not affect the accuracy of the fit, but only scales the coefficients of predictors to be of the same order of magnitude (Scheiplzeth, 2010). To test the individual contribution of each predictor, we compared the full model against all reduced subsets using the F-test (Seber & Lee, 2003), correcting for multiple comparisons using the FDR method.

3. Results

3.1 Meditation increases global differentiation and integration of neural activity

Whole-group within-subject comparison of the conditions revealed that meditative states are characterized by a strong global increase in entropy rate compared to rest. Both LZc and CSER of broadband neural activity show increases ($p<0.001$, after cluster-based correction) in widespread posterior and medial cortical regions (Fig. 2, columns 1 & 2). This finding is in line with accumulating evidence that meditative states are characterized by increased neural complexity compared to resting state (reviewed in Atad et al., 2025). However, these metrics failed to clearly differentiate between the meditative states of self-boundary dissolution (SB-) and maintenance (SB+), with only a small significant cluster for LZc in the temporal cortex (Fig. 2 column 3), although a descriptive trend of increased entropy rate in SB- emerges (Fig. S1). Furthermore, the between-subjects comparison did not yield significant differences between the sub-groups (Fig. S1).

As expected, LZc and CSER showed almost identical results. This finding adds valuable empirical support for the theoretical similarity between both metrics (Mediano et al., 2023). Since LZc and CSER are both estimators of the entropy rate of neural activity and can thus be seen as a proxy for differentiation of neural activity (Mediano et al., 2022; Sarasso et al., 2021), these findings provide convergent evidence that meditation increases global differentiation of neural activity, although broadband entropy rate alone cannot discriminate between self-boundary dissolution and maintenance. Nonetheless, it remains possible that nuanced changes in entropy are accurate predictors of individual phenomenology – as shown in sections 3.2 and 3.3.

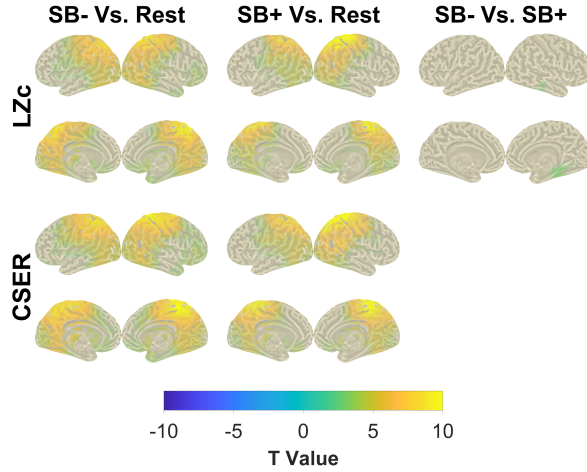


Figure 2. Broadband entropy rate (for both LZc and CSER) increases in meditative states. Inflated cortical surfaces showing source level whole-group condition differences for broadband LZc and CSER. Significant voxels at $p<0.05$ are colored in correspondence to their T-value while non-significant voxels are uncolored.

For information transfer our results show that, compared to rest, meditative states were characterized by increased information transfer for the between-ROIs *pairwise-conditional* (Fig. 3) and within-ROIs *global-conditional* (Fig. 3, top row in each heatmap) analyses. Increases in SB+ vs. rest were more pronounced than SB-, with significant increase in TE primarily from the occipital cortex. Group comparisons show a trend of slightly increased information transfer in SB- for the full dissolvers, from all ROIs excluding the occipital cortex, in which there is a clear trend of decrease (Fig. S2). Within-ROIs *pairwise-conditional* analysis (Fig. S3) yielded mostly mixed results, however a strong differentiation between SB- and SB+ emerges in a specific pattern of reduced information transfer from the anterior cingulate to mid- and post-cingulate (Fig. 4). Interestingly, the between-subjects comparison reveals that in SB+ Vs. Rest the full dissolvers group show the same pattern of reduced anterior cingulate compared to the rest of the group (Fig. S4), indicating perhaps that skillful meditators employ these reductions in meditation generally while others do so only in deeper meditative states.

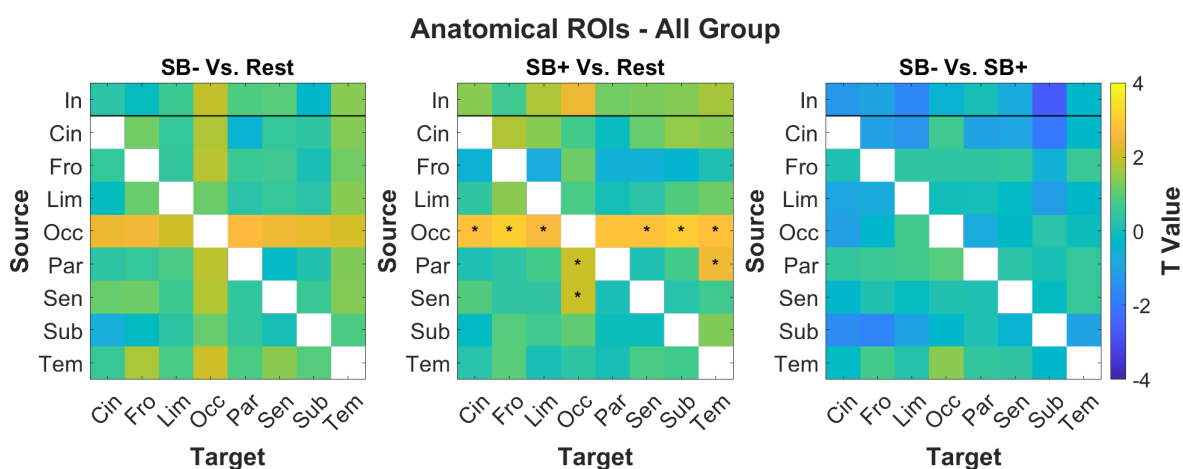


Figure 3. Global information transfer descriptively increases in meditative states. Heatmaps of broadband Transfer Entropy showing whole-group condition differences within and between anatomical ROIs. Significant sub-networks identified through NBS at $p<0.05$ are marked with an asterisk. The top row of each plot labeled “In” corresponds to global-conditional TE within each ROI. ROI abbreviations: Cin - Cingulate, Fro - frontal, Lim - limbic, Occ - occipital, Par - parietal, Sen - sensorimotor, Sub - subcortical, Tem - temporal.

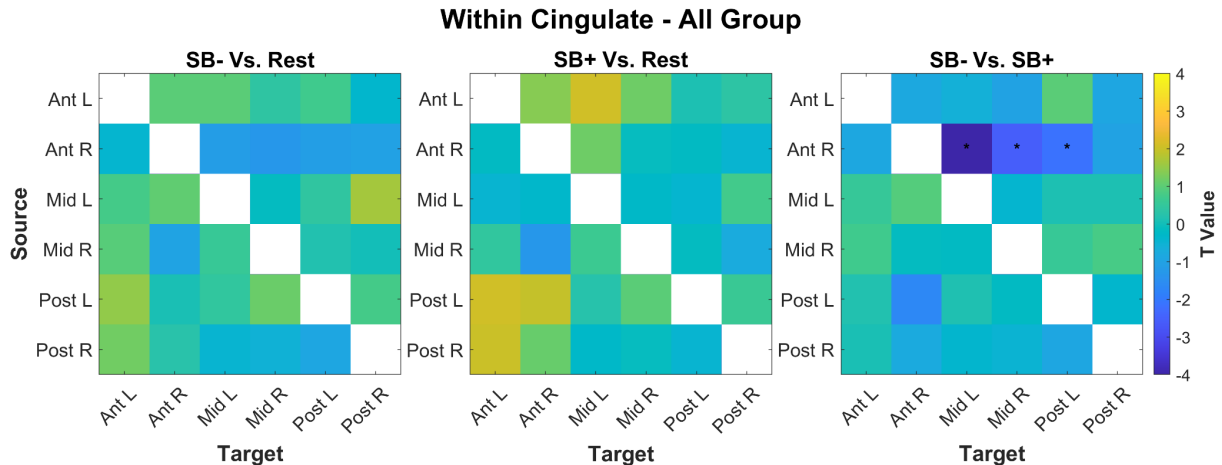


Figure 4. Reduced broadband information transfer from the anterior cingulate to mid- and post-cingulate differentiates SB-dissolution from SB-maintenance meditation. Heatmaps of broadband pairwise-conditional Transfer Entropy showing whole-group condition differences within the cingulate cortex. Significant sub-networks identified through NBS at $p < 0.05$ are marked with an asterisk. Abbreviations: Ant - anterior cingulate, Mid - midcingulate, Post - posterior cingulate. “L” and “R” denote left and right hemispheres.

3.2 Directionality of condition differences is frequency-dependent for entropy rate but not for information transfer

As previously mentioned, TE and CSER allow for a principled decomposition into individual frequency components. To assess whether the observed overall effects are frequency-dependent, we decomposed broadband TE and CSER into canonical frequency bands (Table S1). Spectral decomposition reveals that both broadband TE and CSER effects are mainly driven by high-frequency bands of low and high gamma (Figs. 5,6). Interestingly, although all spectral components change in the same direction for TE (Figs. 6, S5), the results for CSER are nuanced: not only the magnitude of contribution to the total effects, but also the directionality of changes in entropy rate between experimental conditions is frequency-dependent (Fig. 5). Compared to rest, meditative states exhibit increases in entropy rate in low frequencies (delta, theta bands) and high frequencies (low and high gamma bands), while for alpha and low beta bands entropy rate is lower in meditative state than rest and the high beta band exhibits mixed effects (Fig. 5, bottom panel). Furthermore, the spectral decomposition reveals differences between the meditative conditions not captured by broadband entropy rate- namely slight increases in CSER in SB- Vs. SB+, mainly in sensorimotor areas, in theta and high gamma bands, and robust decreases in SB- Vs. SB+ in sensorimotor and posterior-medial cortices for high beta (Fig. 5, bottom panel). Interestingly, the decreases in CSER in high beta are almost identical in spatial location to the whole-group effect of high beta spectral power decreases in previous analysis (see Fig. S3 in Trautwein et al., 2024).

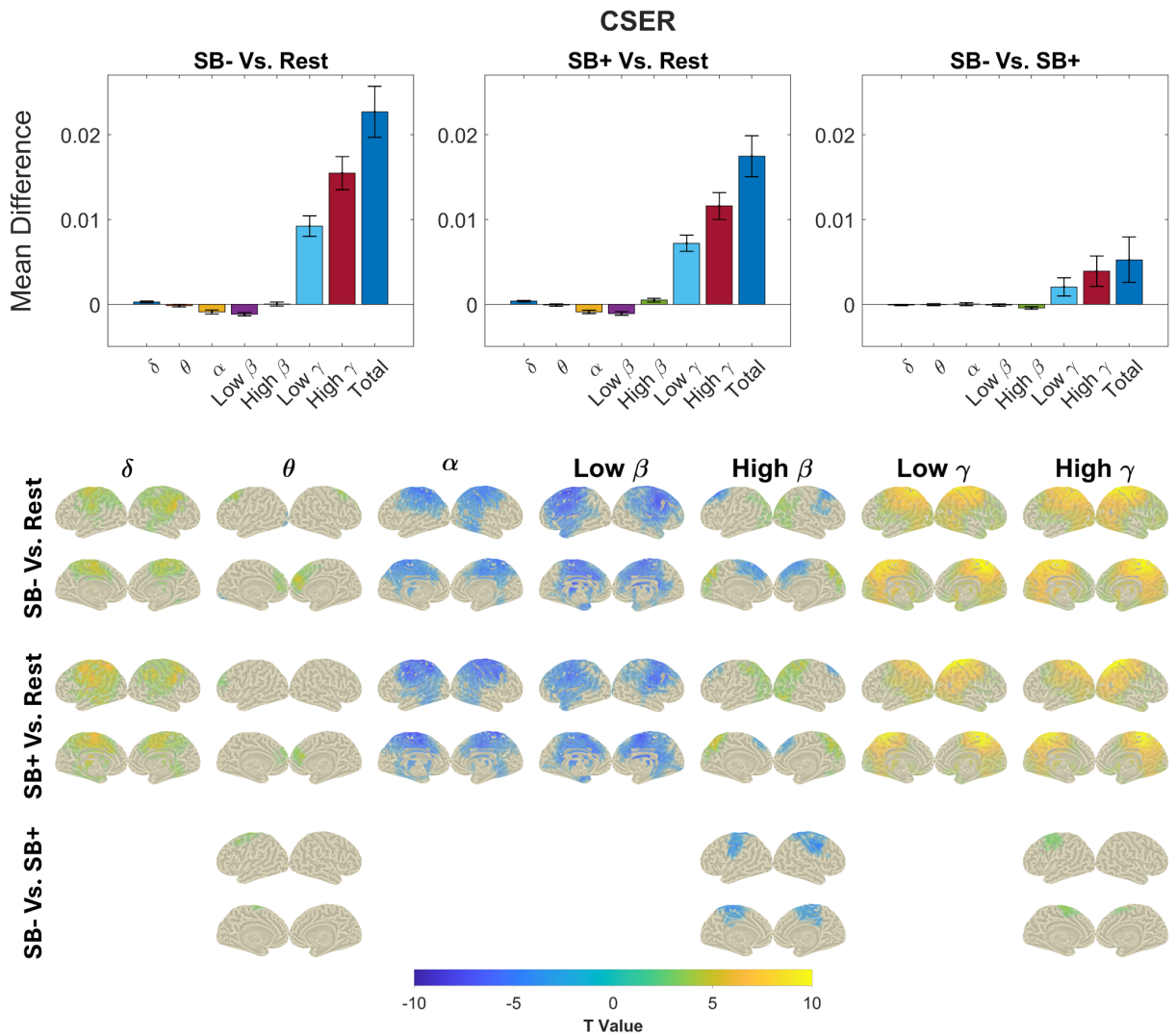


Figure 5. Entropy rate is driven by high frequencies, directionality of condition differences is frequency-dependent.

Top panel: Mean difference in CSER between experimental conditions across all voxels in each frequency band, with standard error of the mean. By definition, band values sum up to the total broadband value. **Bottom panel:** Inflated cortical surfaces showing source level whole-group condition differences for spectrally-decomposed CSER. Significant voxels at $p < 0.05$ are colored in correspondence to their T-value while non-significant voxels are uncolored.

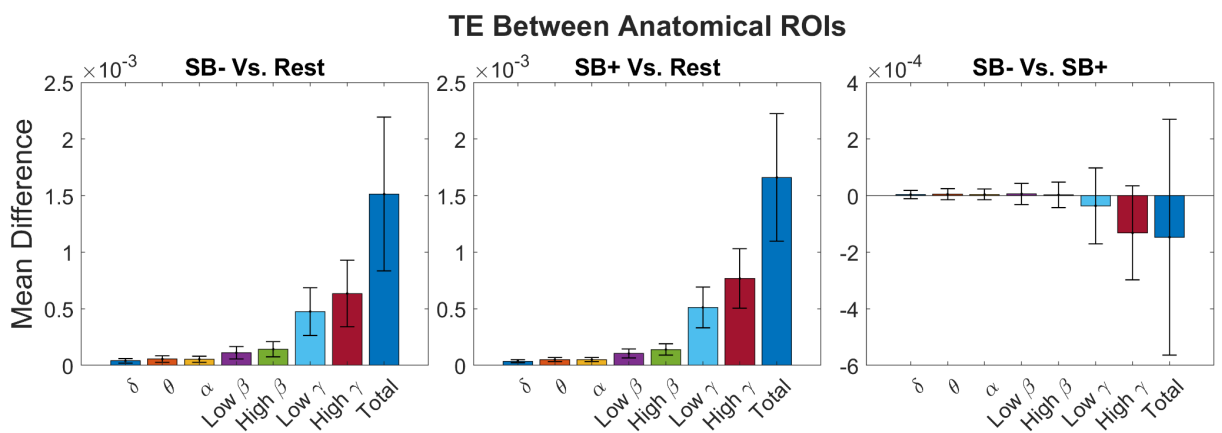


Figure 6. Information is driven by high frequencies. Mean difference in between-ROIs TE between experimental conditions network nodes in each frequency band, with standard error of the mean. By definition, band values sum up to the total broadband value. Note that for visualization purposes, the SB- Vs. SB+ plot has a different y-axis scale.

3.3 Neural correlates of self-dissolution phenomenology

So far, we have found that entropy and information transfer reflect global changes in neural dynamics in meditation compared to rest, yet don't clearly discriminate between the meditative states (SB+ and SB-), questioning their usefulness for understanding self-dissolution phenomenology or MPE-like states. Next, we show that this is not the case- via employing neurophenomenology, it becomes evident that nuanced changes in entropy rate and information transfer are good predictors of self-dissolution phenomenology at the individual level.

Whole-group correlations ($N=44$, see methods) of neural measures with dissolution phenomenology show that a decrease in LZc in orbitofrontal cortex between SB- and SB+ (Fig. 7 A-C) is strongly correlated with DDC, ($r = -0.57$, $p = 0.0304$, cluster-corrected, $q = 0.0456$, cluster- and FDR-corrected). Furthermore, decreases in TE from the cingulate, occipital, limbic and subcortical areas between SB- and SB+ (Fig. 7 D-F) strongly correlate with DDC ($r = -0.50$, $p = 0.0098$, NBS-corrected, $q = 0.0294$, NBS- and FDR-corrected). Importantly, these strong neural correlates, showing specific decreases in SB- Vs. SB+, should be understood in the context of the global increases seen in the rest of the brain in the meditative states compared to rest. While meditation induces global increases in differentiation and integration, participants who reached full-fledged SB-dissolution showed a nuanced pattern of decreases in these areas while in less skillful participants, these areas followed the general pattern of global increases (see barplots- Fig. 7 C,F).

Given the positive results of these univariate predictors, we next ask whether the combination of these neural correlates predicts dissolution phenomenology over and above each of the correlates separately. To answer this question, we fitted a multiple linear regression model predicting dissolution scores from neural differences between SB- and SB+ meditation conditions from the individually predictive regions found here (Fig. 7 A-F), alongside the pre-computed neural correlate of high-beta reductions in posterior-medial cortex (Fig. 7 G-I, see Trautwein et al., 2024 for the original presentation). Indeed, our combined model reaches exceptionally strong predictive power, explaining above 52% of the variance in dissolution scores with an average prediction error of 0.195 on a 0–1 scale ($R^2 = 0.523$, RMSE = 0.195) (Fig. 7J, Table S3). When comparing the full model against all reduced subsets (Table 1), the full model explained significantly more variance than any single or two-predictor model ($\Delta R^2 = 0.093\text{--}0.406$, all FDR-corrected $p \leq 0.008$). This indicates a synergistic effect, in which reductions of high-beta in posterior-medial cortex, orbitofrontal cortex LZc reductions, and reductions in TE from the cingulate, occipital, limbic and subcortical areas, jointly predict dissolution phenomenology.

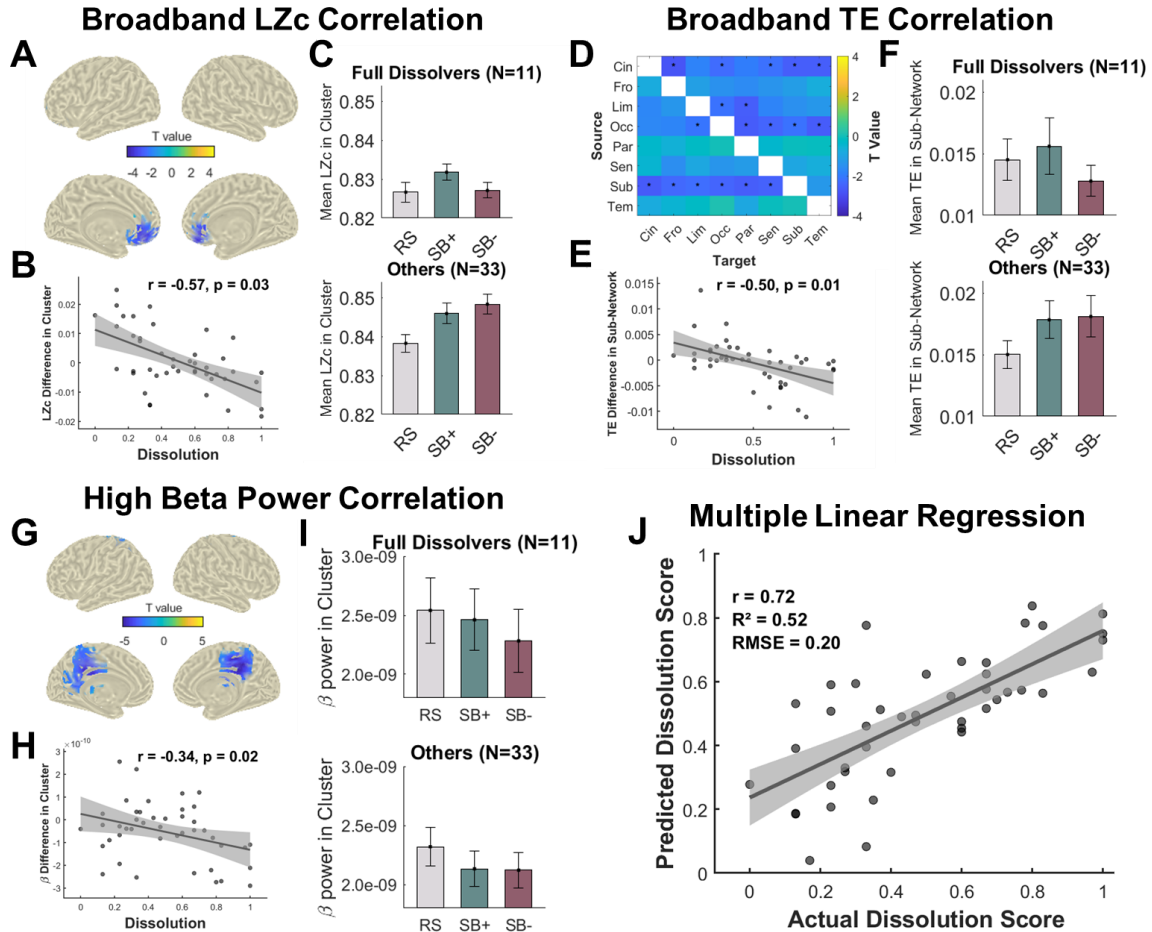


Figure 7. Specific reductions in SB- vs SB+ strongly correlate with dissolution phenomenology. **Top left panel:** broadband LZc correlation. **A:** inflated cortical surface of significant region where LZc SB- vs. SB+ difference correlates with dissolution. **B:** scatterplot showing mean LZc difference in the significant cluster per subject, with p-value taken from the cluster test. The regression line is plotted in black with 95% confidence interval in gray. **C:** barplot of mean LZc in the cluster with standard error of the mean in the cluster for all of the 3 conditions. **Top right panel:** broadband TE between-ROIs correlation. **D:** heatmap of t-values for the correlation of TE with dissolution, significant sub-networks are marked with an asterisk. ROI abbreviations: Cin - Cingulate, Fro - frontal, Lim - limbic, Occ - occipital, Par - parietal, Sen - sensorimotor, Sub - subcortical, Tem - temporal. **E:** scatterplot showing mean TE difference in the significant sub-network, with p-value taken from the NBS test. The regression line is plotted in black with 95% confidence interval in gray. **F:** barplot of mean TE in the significant sub-network, with standard error of the mean for all of the 3 conditions. **Bottom left panel:** high-beta correlation adapted from Trautwein et al. (2024). **G:** inflated cortical surface of significant region where high beta SB- vs. SB+ difference correlates with dissolution. **H:** scatterplot showing mean high beta difference in the significant cluster per subject. The regression line is plotted in black with 95% confidence interval in gray. **I:** barplot of mean high beta in the cluster with standard error of the mean in the cluster for all of the 3 conditions. **Bottom right panel:** **J:** Multiple linear regression using SB-, SB+ difference values of the 3 neural correlates (z-scored) as predictors of dissolution phenomenology. Notice that the linear model takes each predictor with a minus sign and therefore the slope of the regression line is positive. The correlation value (r), equivalent to the square root of R^2 , is also reported for consistency with previous correlation plots. The regression line is plotted in black with 95% confidence interval in gray.

Model Comparison	F	ΔR^2	p (FDR-corrected)
Full Vs. Beta-only (LZc and TE added)	17.03	0.406	<.001
Full Vs. LZc-only (Beta and TE added)	8.52	0.203	0.001
Full Vs. TE-only (Beta and LZc added)	11.32	0.270	<0.001
Full Vs. Beta+LZc (TE added)	8.51	0.102	0.007
Full Vs. Beta+TE (LZc added)	14.32	0.171	0.001
Full Vs. LZc+TE (Beta added)	7.8	0.093	0.008

Table 1. F-tests for comparing the full model with all possible subsets reveal a synergistic effect for the neural correlates of dissolution phenomenology. Column 1: subset comparison. Column 2: F-score. Column 3: difference in explained variance between the full model and the tested subset. Column 4: FDR-corrected p-value for the F-test.

4. Discussion

Capitalizing on a unique large-scale neurophenomenological dataset, we asked how different meditative states affect the information dynamics of neural activity and if observed changes can explain self-boundary (SB) dissolution phenomenology. We build on thick phenomenological (Berkovich-Ohana et al., 2020) data and on an active-control meditation condition to pinpoint neural changes specifically associated with SB-dissolution. Since attenuation of the self construct is a central aspect of MPE-like states, our findings provide insights into the neural dynamics underlying such profound alterations in consciousness. Our comprehensive analysis reveals that meditative SB-dissolution involves a complex interplay of global neural changes and selective regional modulations. Alongside previously established reductions in spectral power in most bands, and most prominently in high-beta in the posterior-medial cortex (Trautwein et al., 2024), neural complexity measures illustrate an intriguing pattern of changes. While meditation generally increases both broadband neural entropy rate and directed information transfer, deeper SB-dissolution states are mainly characterized by further specific patterns of reduction. These specific reductions include reduced broadband information transfer from the anterior to the mid- and post- cingulate cortex, reduced sensorimotor and posterior-medial high-beta entropy rate, reduced broadband information transfer from cingulate, limbic, occipital and subcortical areas, and reduced broadband entropy rate in the orbitofrontal cortex. The specific broadband reductions in information transfer and entropy correlate strongly with dissolution phenomenology ($r = -0.5$, $r = -0.57$, respectively), and when combined with the previously established correlate of reductions in posterior-medial high beta power in a multiple linear regression, produce an unprecedented synergistic prediction of MPE-like phenomenology ($R^2 = 0.52$), which demonstrates the multi-faceted nature of self-dissolution and establishes a uniquely powerful neurophenomenological association.

Following, we discuss the global effects of meditation on neural complexity, emphasizing the novelty of our findings in information transfer (section 4.1); we then examine the neural correlates of self-boundary dissolution, detailing how our neurophenomenological analysis identified specific neural signatures that differentiate these states (section 4.2); finally, we consider the implications of our results for computational phenomenology and active inference accounts of minimal phenomenal experience and deep meditative states (section 4.3), concluding with limitations and future directions (section 4.4).

4.1 Global effects of meditation on neural complexity

Our analyses reveal that meditative states induce global increases in broadband entropy rate and information transfer compared to rest, suggesting enhanced differentiation and integration of neural activity. Increases in entropy rate in meditative states are aligned with a growing body of literature (Atad et al., 2025) reporting a similar trend. Spectral decomposition reveals that entropy rate effects are strongly driven by high-frequency activity (low and high gamma bands, 30-100 Hz). This result replicates findings across various conscious states (Mediano et al., 2023), thus suggesting an inherent feature of these measures rather than a meditation-specific phenomenon. Entropy rate in low-frequency (delta, theta) and high-frequency bands (low and high gamma) is higher in meditative states compared to rest, while middle-range frequency bands (alpha, low beta) show decreases or mixed effects (high beta). This frequency-specific pattern provides important refinement to the common treatment of broadband entropy rate as a unitary phenomenon in consciousness research.

Our findings on increased information transfer in meditation represent a novel contribution to the field, as directed information transfer during meditative states has received limited empirical attention. These results align with and add nuance to more established findings of increased global integration as shown in various non-directed connectivity measures (Tripathi et al., 2025; van Luterveld et al., 2017). Interestingly, unlike the similarity of entropy rate increases in both meditative and psychedelic states (Atad et al., 2025), our results of increased information transfer show an opposite effect compared to psychedelics, where information transfer is reduced in comparison to placebo (Barnett et al., 2020; Rajpal et al., 2022). This divergence offers a unique opportunity to differentiate between these two prominent altered states of consciousness on a mechanistic level, as elaborated in section 4.3.

4.2 Neural correlates of self-boundary dissolution in meditation

While global effects failed to distinguish between self-boundary dissolution (SB-) and maintenance (SB+) conditions, our neurophenomenological analysis revealed specific neural signatures that differentiate these states, alongside specific neural correlates of dissolution phenomenology.

First, the group level effects significantly differentiating SB- from SB+ include reduced high-beta entropy rate in posterior-medial and sensorimotor cortices, alongside slight increases in high-gamma entropy rate in sensorimotor cortex. Interestingly, the spatial distribution of high-beta entropy rate reductions closely mirrors the whole-group effects of high-beta spectral power reductions previously reported in this dataset (Trautwein et al., 2024), demonstrating convergence between spectral power and complexity measures. This convergence strengthens the interpretation that high-beta oscillations in posterior-medial cortex represent a fundamental neural signature of the minimal self, consistent with work linking beta oscillations to the maintenance of top-down predictions precision estimates and gamma oscillations to the bottom-up signaling of prediction error (Bastos et al., 2012; Bauer et al., 2014; Friston et al., 2015). In line with this, increased high-gamma entropy rate in the sensorimotor cortex may reflect an increase in prediction error rate of sensory stimuli, when not suppressed by body related predictions.

Second, on the group level, reduced broadband information transfer from the anterior cingulate to mid-and post cingulate significantly differentiated SB- from SB+. The anterior cingulate cortex plays central roles in cognitive control, conflict monitoring, and self-referential processing (Bush et al., 2000; Northoff & Bermpohl, 2004), making its reduced influence during self-dissolution theoretically coherent, and reflective of the observed phenomenology of “letting go” (Nave et al., 2021). This

finding suggests that the suspension of self-boundaries may involve a relaxation of top-down control mechanisms originating from regions critical for maintaining coherent self-representation, and a relaxation of cognitive control. This is aligned with the hypofrontality theory, which proposes that many altered states of consciousness arise from reduced activity in frontal brain regions, especially the prefrontal cortex, diminishing top-down control and self-referential processing (Dietrich, 2003). The finding regarding a similar pattern for SB+ in the full dissolvers, suggests that skillful meditators already employ this relaxation in more general forms of meditation, while the others rely on this mechanism for the transition to self-dissolution meditation. As broadband TE effects are strongly driven by gamma-band activity which is related to bottom-up signaling of prediction error (Bastos et al., 2012; Bauer et al., 2014; Friston et al., 2015), one mechanism of SB-dissolution - compared to the control meditative state - may be a reduction in information transfer of prediction errors from anterior to posterior cingulate regions.

Third, when incorporating of interindividual differences in phenomenology into the analysis, a strong differentiation becomes evident, where alongside global increases in entropy rate and information transfer in the meditative states, a relative reduction of specific neural features strongly correlates with dissolution phenomenology (Fig. 7). The correlation between relative reduction of entropy rate in the orbitofrontal cortex (OFC) and dissolution depth provides novel insights into the neural mechanisms of self-boundary dissolution. The OFC is classically associated with valuation, reward processing, and flexible updating of stimulus-outcome associations (Rolls, 2000; Kringelbach & Rolls, 2004; Rushworth et al., 2011; Wallis, 2007) and representation of self-referential stimuli (Northoff & Bermpohl, 2004). More recently, the OFC has been framed within predictive coding accounts as a hub for generating and updating predictions about the affective and motivational significance of sensory inputs (Barrett & Simmons, 2015; Wilson et al., 2014). Our finding that entropy rate in the OFC is reduced during successful dissolution compared to the active control meditation thus suggests that there might also be a subtle affective component in SB-dissolution, and specifically, that the suspension of self-evidencing loops and rushing prediction errors does not lead to updating of affective-motivational predictions in these practitioners. Based on the previously reported association between lifetime meditation practice and dissolution depth (Nave et al., 2021), it can be speculated that this is due to a higher familiarity with (and acceptance) of the related neural state-space. While positive affective valence during SB- was not related with phenomenological dissolution depth, it has been related to enhanced self-death acceptance (Dor-Ziderman et al., 2025). Future studies might zoom into the putatively more fine-grained affective meaning of these effects.

Similarly, while information transfer in meditative states generally increases, a reduction of information transfer from occipital, cingulate, limbic and subcortical areas strongly correlates with SB-dissolution phenomenology. The reduction of information transfer from the occipital cortex thus possibly relates to decreased emphasis on visual processing and external sensory engagement. The relative reduction of information transfer from cingulate, limbic and subcortical areas during SB- might suggest a gating of bodily signals from deeper brain regions, previously related to phenomenologically reduced sense of time and space (Berkovich-Ohana et al., 2013).

Finally, we have shown that when taken together, the neural correlates we have found in addition to reduction in posterior-medial cortex high-beta power found in the previous study, yielded a remarkably strong predictive model, explaining over half the variance in phenomenological dissolution scores. This uniquely powerful effect, alongside the significant contributions of each of the three neural correlates to the predictive model, suggest that self-boundary dissolution is a synergistic phenomenon reflected across multiple scales and aspects of neural dynamics. This

multi-faceted neural signature aligns with phenomenological accounts of self-dissolution as an emergent property arising from the dynamic interplay of distributed processes (Berkovich-Ohana et al., 2024), rather than being localized to specific brain regions (Giommi et al., 2023).

4.3 Implications for computational phenomenology and active inference accounts of MPE and deep meditative states

Our findings have important implications for computational phenomenology and active inference accounts of deep meditative states, particularly with regard to how self-boundary (SB) dissolution can be understood as a reconfiguration of precision-weighted priors and prediction error signaling. Several recent accounts converge on a framing of progressively deep meditative states as involving a loosening of top-down constraints, reflected in the progressive reduction of prior precisions (Laukkonen & Slagter, 2021; Mago et al., 2024; Pagnoni, 2019; Prest & Berryman, 2024, reviewed in Tal et al., 2025). In predictive coding terms, reducing prior precision makes top-down predictions less dominant in shaping perception; when priors lose precision, the brain treats them as less reliable, so bottom-up sensory evidence (prediction error) gains more influence on updating the generative model. Crucially, the observation that global increases in complexity accompany meditation in general, but that selective reductions in entropy and information transfer specifically track SB-dissolution, provides a mechanistically precise way to test active inference accounts: it shows how meditation can simultaneously enhance the richness of neural dynamics while locally suspending information flow that sustains the self-model. Recent advances in neurophenomenology further suggest that phenomenological categories can be formulated within computational models such as the active inference framework (Ramstead et al., 2022). Such approaches provide a formalized bridge between phenomenal and neural domains (Lutz et al., 2025) and have specifically been applied to advanced meditative states, including pure awareness or MPE states (Mago et al., 2024, Sandved-Smith, 2024). Our results contribute to this endeavor by demonstrating how global and selective neural complexity modulations jointly map onto the phenomenology of SB-dissolution, offering a refined computational account of how the predictive mind reorganizes in profound meditative states.

Our findings of global increases in entropy rate generally validate accounts of reduced top-down control (Laukkonen & Slagter, 2021), yet add nuance to these. Importantly, however, they challenge predictions that deep meditative states entail a global increase in entropy (Mago et al., 2024). Mago and colleagues argue that MPE states arise when precision weighting is shifted toward lower levels of a hierarchical inference system, producing a perceptual state with increased entropy and reduced complexity. Instead, we show that dissolution is characterized by specific reductions in entropy and information transfer against a globally elevated baseline—suggesting a more nuanced process of selective suppression rather than uniform “entropy maximization.” Our results thus call for a refinement of the hypothesis of a global “flattening” of predictive hierarchies (Laukkonen & Slagter, 2021) suggesting that this “flattening” occurs across some phenomenal dimensions, that are reflected in specific neural circuits.

Reduced information transfer from the anterior to mid- and posterior cingulate explicitly supports predictions from computational phenomenology regarding the neural mechanism of effortlessness in MPE (Sandved-Smith, 2024), and aligns with phenomenological reports of “letting go” in dissolution (Metzinger, 2024; Nave, 2021). Taken together, these results suggest that the suspension of self-boundaries is not simply an entropic expansion but involves finely tuned reconfigurations of precision-weighting across hierarchies.

In addition, our results offer a unique opportunity to differentiate between deep meditative states and psychedelics on a mechanistic level, despite both being associated with SB-dissolution phenomenologically (Letheby & Gerrans, 2017; Milliere et al., 2018). The Relaxed Beliefs Under Psychedelics framework (REBUS, Carhart-Harris & Friston, 2019) proposes that psychedelics reduce the precision of high-level priors, allowing a flood of bottom-up prediction errors that destabilize the self-model and open perception to novel interpretations. Meditation accounts (Laukkonen & Slagter, 2021) suggest a gradual attenuation of predictive hierarchies. Our result of increased global information transfer in meditation alongside specific reductions as opposed to the global reductions seen in psychedelics, together with the similarity of increased global entropy rate support an interpretation may suggest that while both involve self-boundary dissolution through altered precision weighting, psychedelics increase perceptual diversity and entropy, whereas meditation drives dynamics toward simplicity and stability.

4.4 Limitations and future directions

While our study leverages a unique large-scale neurophenomenological MEG dataset, several limitations should be noted. First, our analyses are correlational, so causal inferences about the role of specific neural dynamics in self-boundary dissolution remain tentative. Second, although our dataset includes an active-control meditation condition, the generalizability of findings to other meditation traditions, levels of expertise, or non-meditative MPE states remains to be established. Third, while MEG provides excellent temporal resolution, localization of deep or subcortical sources is still limited, and complementary imaging modalities (e.g., fMRI) could further clarify subcortical contributions. Future work could integrate computational modeling to explicitly link observed entropy and information transfer patterns to manipulations of prior precision and prediction error within hierarchical generative models, providing a stronger test of active inference accounts. Longitudinal designs tracking the acquisition of meditative skill would clarify how the observed neural patterns evolve with practice, and experimental manipulations, such as targeted perturbations of network activity or neurofeedback, could probe the causal role of specific hubs (e.g., anterior/posterior cingulate, OFC) in SB-dissolution. Finally, extending these analyses to compare meditation and psychedelics under controlled conditions would illuminate mechanistic similarities and divergences between distinct routes to self-boundary dissolution. Collectively, these directions offer a roadmap for refining mechanistic accounts of deep meditative states and their neural signatures.

5. Conclusion

Our comprehensive analysis reveals that meditative self-boundary dissolution involves a complex interplay of global neural changes and selective regional modulations. While meditation generally increases both neural complexity and information transfer, deeper dissolution states are characterized by nuanced patterns of reduction. The synergistic prediction of phenomenology by multiple neural measures ($R^2 = 0.52$) demonstrates the multi-faceted nature of self-dissolution. Importantly, these results establish a uniquely powerful neurophenomenological association, highlighting the power of using neurophenomenology when studying subtle states of consciousness and selfhood (Varela et al., 1991). These findings advance our understanding of how the brain constructs and, vice versa, can suspend the minimal sense of self, providing empirical constraints for computational models of consciousness and offering insights into the neural basis of deep meditative and MPE-like states.

Bibliography

- Aamodt, A., Sevenius Nilsen, A., Markhus, R., Kusztor, A., HasanzadehMoghadam, F., Kauppi, N., Thürer, B., Storm, J. F., & Juel, B. E. (2023). EEG Lempel-Ziv complexity varies with sleep stage, but does not seem to track dream experience. *Frontiers in Human Neuroscience*, 16. <https://doi.org/10.3389/fnhum.2022.987714>
- Agnorelli, C., Cinti, A., Barillà, G., Lomi, F., Scoccia, A., Benelli, A., Neri, F., Smeralda, C. L., Cuomo, A., Santarneccchi, E., Tatti, E., Godfrey, K., Tarantino, F., Fagiolini, A., & Rossi, S. (2025). Neurophysiological correlates of ketamine-induced dissociative state in bipolar disorder: Insights from real-world clinical settings. *Molecular Psychiatry*, 30(7), 2848–2859. <https://doi.org/10.1038/s41380-025-02889-2>
- Alcaraz-Sánchez, A. (2023). Awareness in the void: A micro-phenomenological exploration of conscious dreamless sleep. *Phenomenology and the Cognitive Sciences*, 22(4), 867–905. <https://doi.org/10.1007/s11097-021-09743-0>
- Amigó, J. M., Szczepański, J., Wajnryb, E., & Sanchez-Vives, M. V. (2004). Estimating the entropy rate of spike trains via Lempel-Ziv complexity. *Neural Computation*, 16(4), 717–736. <https://doi.org/10.1162/089976604322860677>
- Atad, D. A., Mediano, P. A. M., Rosas, F. E., & Berkovich-Ohana, A. (2025). Meditation and complexity: A review and synthesis of evidence. *Neuroscience of Consciousness*, 2025(1), niaf013. <https://doi.org/10.1093/nc/niaf013>
- Ataria, Y., Dor-Ziderman, Y., & Berkovich-Ohana, A. (2015). How does it feel to lack a sense of boundaries? A case study of a long-term mindfulness meditator. *Consciousness and Cognition*, 37, 133–147.
- Barnett, L., Barrett, A. B., & Seth, A. K. (2009). Granger Causality and Transfer Entropy Are Equivalent for Gaussian Variables. *Physical Review Letters*, 103(23), 238701. <https://doi.org/10.1103/PhysRevLett.103.238701>
- Barnett, L., Muthukumaraswamy, S. D., Carhart-Harris, R. L., & Seth, A. K. (2020). Decreased directed functional connectivity in the psychedelic state. *NeuroImage*, 209, 116462. <https://doi.org/10.1016/j.neuroimage.2019.116462>
- Barnett, L., & Seth, A. K. (2014). The MVGC multivariate Granger causality toolbox: A new approach to Granger-causal inference. *Journal of Neuroscience Methods*, 223, 50–68. <https://doi.org/10.1016/j.jneumeth.2013.10.018>
- Barnett, L., & Seth, A. K. (2015). Granger causality for state-space models. *Physical Review E*, 91(4), 040101. <https://doi.org/10.1103/PhysRevE.91.040101>
- Barrett, L. F., & Simmons, W. K. (2015). Interoceptive predictions in the brain. *Nature Reviews Neuroscience*, 16(7), 419–429. <https://doi.org/10.1038/nrn3950>

Bastos, A. M., Usrey, W. M., Adams, R. A., Mangun, G. R., Fries, P., & Friston, K. J. (2012). Canonical microcircuits for predictive coding. *Neuron*, 76(4), 695–711. <https://doi.org/10.1016/j.neuron.2012.10.038>

Bauer, M., Stenner, M.-P., Friston, K. J., & Dolan, R. J. (2014). Attentional modulation of alpha/beta and gamma oscillations reflect functionally distinct processes. *The Journal of Neuroscience: The Official Journal of the Society for Neuroscience*, 34(48), 16117–16125. <https://doi.org/10.1523/JNEUROSCI.3474-13.2014>

Benjamini, Y., & Hochberg, Y. (1995). Controlling the False Discovery Rate: A Practical and Powerful Approach to Multiple Testing. *Journal of the Royal Statistical Society: Series B (Methodological)*, 57(1), 289–300. <https://doi.org/10.1111/j.2517-6161.1995.tb02031.x>

Berkovich-Ohana, A., Brown, K. W., Gallagher, S., Barendregt, H., Bauer, P., Giommi, F., Nyklíček, I., Ostafin, B., Raffone, A., Slagter, H. A., Trautwein, F.-M., Vago, D., & Amaro, A. (2024). Pattern Theory of Selflessness: How Meditation May Transform the Self-Pattern. *Mindfulness*, 15(8), 2114–2140. <https://doi.org/10.1007/s12671-024-02418-2>

Berkovich-Ohana, A., Dor-Ziderman, Y., Glicksohn, J., & Goldstein, A. (2013). Alterations in the sense of time, space, and body in the mindfulness-trained brain: A neurophenomenologically-guided MEG study. *Frontiers in Psychology*, 4. <https://doi.org/10.3389/fpsyg.2013.00912>

Berkovich-Ohana, A., Dor-Ziderman, Y., Trautwein, F.-M., Schweitzer, Y., Nave, O., Fulder, S., & Ataria, Y. (2020). The Hitchhiker's Guide to Neurophenomenology – The Case of Studying Self Boundaries With Meditators. *Frontiers in Psychology*, 11, 1680. <https://doi.org/10.3389/fpsyg.2020.01680>

Blanke, O. (2012). Multisensory brain mechanisms of bodily self-consciousness. *Nature Reviews Neuroscience*, 13(8), 556–571.

Blanke, O., & Metzinger, T. (2009). Full-body illusions and minimal phenomenal selfhood. *Trends in Cognitive Sciences*, 13(1), 7–13.

Boszomaier, T., Barnett, L., Harré, M., & Lizier, J. T. (2016). Transfer Entropy. In T. Boszomaier, L. Barnett, M. Harré, & J. T. Lizier (Eds.), *An Introduction to Transfer Entropy: Information Flow in Complex Systems* (pp. 65–95). Springer International Publishing. https://doi.org/10.1007/978-3-319-43222-9_4

Bush, G., Luu, P., Posner, M. I., Bush, G., Luu, P., Posner, M. I., Bush, G., Luu, P., & Posner, M. I. (2000). Cognitive and emotional influences in anterior cingulate cortex. *Trends in Cognitive Sciences*, 4(6), 215–222. [https://doi.org/10.1016/S1364-6613\(00\)01483-2](https://doi.org/10.1016/S1364-6613(00)01483-2)

Carhart-Harris, R. L., & Friston, K. J. (2019). REBUS and the Anarchic Brain: Toward a Unified Model of the Brain Action of Psychedelics. *Pharmacological Reviews*, 71(3), 316–344. <https://doi.org/10.1124/pr.118.017160>

Christoff, K., Cosmelli, D., Legrand, D., & Thompson, E. (2011). Specifying the self for cognitive neuroscience. *Trends in Cognitive Sciences*, 15(3), 104–112.

Dahl, C. J., Lutz, A., & Davidson, R. J. (2015). Reconstructing and deconstructing the self: Cognitive mechanisms in meditation practice. *Trends in Cognitive Sciences*, 19(9), 515–523. <https://doi.org/10.1016/j.tics.2015.07.001>

Damasio, A. R. (1999). *The feeling of what happens: Body and emotion in the making of consciousness*. Harcourt Brace.

D'Andrea, A., Croce, P., O'Byrne, J., Jerbi, K., Pascarella, A., Raffone, A., Pizzella, V., & Marzetti, L. (2024). Mindfulness meditation styles differently modulate source-level MEG microstate dynamics and complexity. *Frontiers in Neuroscience*, 18. <https://doi.org/10.3389/fnins.2024.1295615>

Dietrich, A. (2003). Functional neuroanatomy of altered states of consciousness: The transient hypofrontality hypothesis. *Consciousness and Cognition*, 12(2), 231–256. [https://doi.org/10.1016/S1053-8100\(02\)00046-6](https://doi.org/10.1016/S1053-8100(02)00046-6)

Dor-Ziderman, Y., Ataria, Y., Fulder, S., Goldstein, A., & Berkovich-Ohana, A. (2016). Self-specific processing in the meditating brain: A MEG neurophenomenology study. *Neuroscience of Consciousness*, 2016(1), niw019. <https://doi.org/10.1093/nc/niw019>

Dor-Ziderman, Y., Berkovich-Ohana, A., Glicksohn, J., & Goldstein, A. (2013). Mindfulness-induced selflessness: A MEG neurophenomenological study. *Frontiers in Human Neuroscience*, 7. <https://www.frontiersin.org/articles/10.3389/fnhum.2013.00582>

Dor-Ziderman, Y., Schweitzer, Y., Nave, O., Trautwein, F.-M., Fulder, S., Lutz, A., Goldstein, A., & Berkovich-Ohana, A. (2025). Training the embodied self in its impermanence: Meditators evidence neurophysiological markers of death acceptance. *Neuroscience of Consciousness*, 2025(1), niaf002. <https://doi.org/10.1093/nc/niaf002>

Friston, K. J., Bastos, A. M., Pinotsis, D., & Litvak, V. (2015). LFP and oscillations—What do they tell us? *Current Opinion in Neurobiology*, 31, 1–6. <https://doi.org/10.1016/j.conb.2014.05.004>

Gallagher, null. (2000). Philosophical conceptions of the self: Implications for cognitive science. *Trends in Cognitive Sciences*, 4(1), 14–21. [https://doi.org/10.1016/s1364-6613\(99\)01417-5](https://doi.org/10.1016/s1364-6613(99)01417-5)

Gallagher, S. (2013). A Pattern Theory of Self. *Frontiers in Human Neuroscience*, 7. <https://doi.org/10.3389/fnhum.2013.00443>

Gallagher, S., & Zahavi, D. (2005). Phenomenological approaches to self-consciousness. In E.N. Zalta (ed.), *The Stanford Encyclopedia of Philosophy*. Stanford University.

Gamma, A., & Metzinger, T. (2021). The Minimal Phenomenal Experience questionnaire (MPE-92M): Towards a phenomenological profile of “pure awareness” experiences in meditators. *PloS One*, 16(7), e0253694. <https://doi.org/10.1371/journal.pone.0253694>

Giommi, F., Bauer, P. R., Berkovich-Ohana, A., Barendregt, H., Brown, K. W., Gallagher, S., Nyklíček, I., Ostafin, B., Raffone, A., Slagter, H. A., Trautwein, F.-M., & Vago, D. R. (2023). The (In)flexible self: Psychopathology, mindfulness, and neuroscience. *International Journal of Clinical and Health Psychology*, 23(4), 100381. <https://doi.org/10.1016/j.ijchp.2023.100381>

Hannan, E. J., & Deistler, M. (2012). *The Statistical Theory of Linear Systems*. SIAM.

Hillebrand, A., Singh, K. D., Holliday, I. E., Furlong, P. L., & Barnes, G. R. (2005). A new approach to neuroimaging with magnetoencephalography. *Human Brain Mapping*, 25(2), 199–211. <https://doi.org/10.1002/hbm.20102>

James, W. (1890). The stream of consciousness. *Principles of Psychology*, 1, 224–290.

Josipovic, Z. (2014). Neural correlates of nondual awareness in meditation: Neural correlates and nondual awareness. *Annals of the New York Academy of Sciences*, 1307(1), 9–18. <https://doi.org/10.1111/nyas.12261>

Kaspar, F., & Schuster, H. G. (1987). Easily calculable measure for the complexity of spatiotemporal patterns. *Physical Review A*, 36(2), 842–848. <https://doi.org/10.1103/PhysRevA.36.842>

Kringelbach, M. L., & Rolls, E. T. (2004). The functional neuroanatomy of the human orbitofrontal cortex: Evidence from neuroimaging and neuropsychology. *Progress in Neurobiology*, 72(5), 341–372. <https://doi.org/10.1016/j.pneurobio.2004.03.006>

Laukkonen, R. E., & Slagter, H. A. (2021). From many to (n)one: Meditation and the plasticity of the predictive mind. *Neuroscience & Biobehavioral Reviews*, 128, 199–217. <https://doi.org/10.1016/j.neubiorev.2021.06.021>

Legrand, D. (2006). The bodily self: The sensori-motor roots of pre-reflective self-consciousness. *Phenomenology and the Cognitive Sciences*, 5(1), 89–118.

Lempel, A., & Ziv, J. (1976). On the Complexity of Finite Sequences. *IEEE Transactions on Information Theory*, 22(1), 75–81. IEEE Transactions on Information Theory. <https://doi.org/10.1109/TIT.1976.1055501>

Letheby, C., & Gerrans, P. (2017). Self unbound: Ego dissolution in psychedelic experience. *Neuroscience of Consciousness*, 2017(1). <https://doi.org/10.1093/nc/nix016>

Lutz, A., Abdoun, O., Dor-Ziderman, Y., Trautwein, F.-M., & Berkovich-Ohana, A. (2025). An Overview of Neurophenomenological Approaches to Meditation and Their Relevance to Clinical Research. *Biological Psychiatry: Cognitive Neuroscience and Neuroimaging*, 10(4), 411–424. <https://doi.org/10.1016/j.bpsc.2024.11.008>

Lutz, A., Dunne, J., & Davidson, R. (2007). Meditation and the neuroscience of consciousness: An introduction. *Cambridge Handbook of Consciousness*.

Mago, J., Chandaria, S., Miller, M., & Laukkonen, R. (2024). *Pure awareness, entropy, and the foundation of perception*. OSF. https://doi.org/10.31234/osf.io/c7naw_v1

Maris, E., & Oostenveld, R. (2007). Nonparametric statistical testing of EEG- and MEG-data. *Journal of Neuroscience Methods*, 164(1), 177–190. <https://doi.org/10.1016/j.jneumeth.2007.03.024>

Mediano, P. A. M., Rosas, F. E., Bor, D., Seth, A. K., & Barrett, A. B. (2022). The strength of weak integrated information theory. *Trends in Cognitive Sciences*, 26(8), 646–655. <https://doi.org/10.1016/j.tics.2022.04.008>

Mediano, P. A. M., Rosas, F. E., Luppi, A. I., Noreika, V., Seth, A. K., Carhart-Harris, R. L., Barnett, L., & Bor, D. (2023). Spectrally and temporally resolved estimation of neural signal diversity. *eLife*, 12. <https://doi.org/10.7554/eLife.88683.1>

Mediano, P. A. M., Rosas, F. E., Timmermann, C., Roseman, L., Nutt, D. J., Feilding, A., Kaelen, M., Kringlebach, M. L., Barrett, A. B., Seth, A. K., Muthukumaraswamy, S., Bor, D., & Carhart-Harris, R. L. (2024). Effects of External Stimulation on Psychedelic State Neurodynamics. *ACS Chemical Neuroscience*, 15(3), 462–471. <https://doi.org/10.1021/acschemneuro.3c00289>

Metzinger, T. (2003). *Being no one: The self-model theory of subjectivity*. MIT Press.

Metzinger, T. (2020). Minimal phenomenal experience: Meditation, tonic alertness, and the phenomenology of “pure” consciousness. *Philosophy and the Mind Sciences*, 1(I), 1–44. <https://doi.org/10.33735/phimisci.2020.I.46>

Metzinger, T. (2024). *The elephant and the blind: the experience of pure consciousness: philosophy, science, and*

Millière, R., Carhart-Harris, R. L., Roseman, L., Trautwein, F.-M., & Berkovich-Ohana, A. (2018). Psychedelics, Meditation, and Self-Consciousness. *Frontiers in Psychology*, 9. <https://doi.org/10.3389/fpsyg.2018.01475>

Nave, O., Trautwein, F.-M., Ataria, Y., Dor-Ziderman, Y., Schweitzer, Y., Fulder, S., & Berkovich-Ohana, A. (2021). Self-Boundary Dissolution in Meditation: A Phenomenological Investigation. *Brain Sciences*, 11(6), Article 6. <https://doi.org/10.3390/brainsci11060819>

Nikolic, M., Mediano, P., Froese, T., Reydellet, D., & Palenicek, T. (2024). *Psilocybin alters brain activity related to sensory and cognitive processing in a time-dependent manner* (p. 2024.09.09.24313316). medRxiv. <https://doi.org/10.1101/2024.09.09.24313316>

Nolte, G. (2003). The magnetic lead field theorem in the quasi-static approximation and its use for magnetoencephalography forward calculation in realistic volume conductors. *Physics in Medicine & Biology*, 48(22), 3637. <https://doi.org/10.1088/0031-9155/48/22/002>

Northoff, G., & Bermöhl, F. (2004). Cortical midline structures and the self. *Trends in Cognitive Sciences*, 8(3), 102–107. <https://doi.org/10.1016/j.tics.2004.01.004>

Oostenveld, R., Fries, P., Maris, E., & Schoffelen, J.-M. (2011). FieldTrip: Open source software for advanced analysis of MEG, EEG, and invasive electrophysiological data. *Computational Intelligence and Neuroscience*, 2011, 156869. <https://doi.org/10.1155/2011/156869>

Pagnoni, G. (2019). The contemplative exercise through the lenses of predictive processing: A promising approach. *Progress in Brain Research*, 244, 299–322. <https://doi.org/10.1016/bs.pbr.2018.10.022>

Petitmengin, C. (2006). Describing one’s subjective experience in the second person: An interview method for the science of consciousness. *Phenomenology and the Cognitive Sciences*, 5(3), 229–269.

Prest, S., & Berryman, K. (2024). *Towards an Active Inference Account of Deep Meditative Deconstruction*. OSF. <https://doi.org/10.31234/osf.io/d3gpf>

Rajpal, H., Mediano, P. A. M., Rosas, F. E., Timmermann, C. B., Brugger, S., Muthukumaraswamy, S., Seth, A. K., Bor, D., Carhart-Harris, R. L., & Jensen, H. J. (2022). Psychedelics and schizophrenia: Distinct alterations to Bayesian inference. *NeuroImage*, 263, 119624. <https://doi.org/10.1016/j.neuroimage.2022.119624>

Ramstead, M. J. D., Seth, A. K., Hesp, C., Sandved-Smith, L., Mago, J., Lifshitz, M., Pagnoni, G., Smith, R., Dumas, G., Lutz, A., Friston, K., & Constant, A. (2022). From Generative Models to Generative Passages: A Computational Approach to (Neuro) Phenomenology. *Review of Philosophy and Psychology*, 13(4), 829–857. <https://doi.org/10.1007/s13164-021-00604-y>

Ratcliffe, M. (2008). *Feelings of being: Phenomenology, psychiatry and the sense of reality*. Oxford University Press.

Rodriguez-Larios, J., Bracho Montes De Oca, E. A., & Alaerts, K. (2021). The EEG spectral properties of meditation and mind wandering differ between experienced meditators and novices. *NeuroImage*, 245, 118669. <https://doi.org/10.1016/j.neuroimage.2021.118669>

Rolls, E. T. (2000). The Orbitofrontal Cortex and Reward. *Cerebral Cortex*, 10(3), 284–294. <https://doi.org/10.1093/cercor/10.3.284>

Rushworth, M. F. S., Noonan, M. P., Boorman, E. D., Walton, M. E., & Behrens, T. E. (2011). Frontal Cortex and Reward-Guided Learning and Decision-Making. *Neuron*, 70(6), 1054–1069. <https://doi.org/10.1016/j.neuron.2011.05.014>

Sandved-Smith, L. (2024). *A Computational Model of Minimal Phenomenal Experience (MPE)* (2024110649). Preprints. <https://doi.org/10.20944/preprints202411.0649.v1>

Sarasso, S., Casali, A. G., Casarotto, S., Rosanova, M., Sinigaglia, C., & Massimini, M. (2021). Consciousness and complexity: A consilience of evidence. *Neuroscience of Consciousness*, niab023. <https://doi.org/10.1093/nc/niab023>

Schartner, M. M., Carhart-Harris, R. L., Barrett, A. B., Seth, A. K., & Muthukumaraswamy, S. D. (2017). Increased spontaneous MEG signal diversity for psychoactive doses of ketamine, LSD and psilocybin. *Scientific Reports*, 7, 46421. <https://doi.org/10.1038/srep46421>

Schartner, M., Seth, A., Noirhomme, Q., Boly, M., Bruno, M.-A., Laureys, S., & Barrett, A. (2015). Complexity of Multi-Dimensional Spontaneous EEG Decreases during Propofol Induced General Anaesthesia. *PLOS ONE*, 10(8), e0133532. <https://doi.org/10.1371/journal.pone.0133532>

Schielzeth, H. (2010). Simple means to improve the interpretability of regression coefficients. *Methods in Ecology and Evolution*, 1(2), 103–113. <https://doi.org/10.1111/j.2041-210X.2010.00012.x>

Schreiber, T. (2000). Measuring Information Transfer. *Physical Review Letters*, 85(2), 461–464. <https://doi.org/10.1103/PhysRevLett.85.461>

Seber, G. A. F., & Lee, A. J. (2003). Linear Regression Analysis (2nd ed.). Hoboken, NJ: Wiley.

Seth, A. K. (2013). Interoceptive inference, emotion, and the embodied self. *Trends in Cognitive Sciences*, 17(11), 565–573.

Tal, H., Wright, M., Prest, S., Sandved-Smith, L., & Sacchet, M. (2025). *Active Inference, Computational Phenomenology, and Advanced Meditation: Toward the Formalization of the Experience of Meditation*. OSF. https://doi.org/10.31234/osf.io/pm5y2_v2

Thompson, E., Lutz, A., & Cosmelli, D. (2005). Neurophenomenology: An Introduction for Neurophilosophers. In *Cognition and the brain: The philosophy and neuroscience movement* (pp. 40–97). Cambridge University Press. <https://doi.org/10.1017/CBO9780511610608.003>

Timmermann, C., Bauer, P. R., Gosseries, O., Vanhaudenhuyse, A., Vollenweider, F., Laureys, S., Singer, T., Mind and Life Europe (MLE) ENCECON Research Group, Antonova, E., & Lutz, A. (2023). A neurophenomenological approach to non-ordinary states of consciousness: Hypnosis, meditation, and psychedelics. *Trends in Cognitive Sciences*, 27(2), 139–159. <https://doi.org/10.1016/j.tics.2022.11.006>

Timmermann, C., Roseman, L., Schartner, M., Milliere, R., Williams, L. T. J., Erritzoe, D., Muthukumaraswamy, S., Ashton, M., Bendrioua, A., Kaur, O., Turton, S., Nour, M. M., Day, C. M., Leech, R., Nutt, D. J., & Carhart-Harris, R. L. (2019). Neural correlates of the DMT experience assessed with multivariate EEG. *Scientific Reports*, 9(1), 1–13. <https://doi.org/10.1038/s41598-019-51974-4>

Tononi, G., Boly, M., Massimini, M., & Koch, C. (2016). Integrated information theory: From consciousness to its physical substrate. *Nature Reviews Neuroscience*, 17(7), 450–461. <https://doi.org/10.1038/nrn.2016.44>

Tononi, G., & Edelman, G. M. (1998). Consciousness and complexity. *Science*, 282(5395), 1846–1851.

Trautwein, F.-M., Schweitzer, Y., Dor-Ziderman, Y., Nave, O., Ataria, Y., Fulder, S., & Berkovich-Ohana, A. (2024). Suspending the Embodied Self in Meditation Attenuates Beta Oscillations in the Posterior Medial Cortex. *The Journal of Neuroscience: The Official Journal of the Society for Neuroscience*, 44(26), e1182232024. <https://doi.org/10.1523/JNEUROSCI.1182-23.2024>

Tripathi, V., Batta, I., Zamani, A., Atad, D. A., Sheth, S. K. S., Zhang, J., Wager, T. D., Whitfield-Gabrieli, S., Uddin, L. Q., Prakash, R. S., & Bauer, C. C. C. (2025). Default Mode Network Functional Connectivity As a Transdiagnostic Biomarker of Cognitive Function. *Biological Psychiatry: Cognitive Neuroscience and Neuroimaging*, 10(4), 359–368. <https://doi.org/10.1016/j.bpsc.2024.12.016>

Tzourio-Mazoyer, N., Landeau, B., Papathanassiou, D., Crivello, F., Etard, O., Delcroix, N., Mazoyer, B., & Joliot, M. (2002). Automated Anatomical Labeling of Activations in SPM Using a Macroscopic Anatomical Parcellation of the MNI MRI Single-Subject Brain. *NeuroImage*, 15(1), 273–289. <https://doi.org/10.1006/nimg.2001.0978>

van Luterveld, R., van Dellen, E., Pal, P., Yang, H., Stam, C. J., & Brewer, J. (2017). Meditation is associated with increased brain network integration. *NeuroImage*, 158, 18–25. <https://doi.org/10.1016/j.neuroimage.2017.06.071>

Van Veen, B. D., Van Drongelen, W., Yuchtman, M., & Suzuki, A. (1997). Localization of brain electrical activity via linearly constrained minimum variance spatial filtering. *IEEE Transactions on*

Biomedical Engineering, 44(9), 867–880. IEEE Transactions on Biomedical Engineering. <https://doi.org/10.1109/10.623056>

Varela, F. J., Thompson, E., & Rosch, E. (1991). *The embodied mind: Cognitive science and human experience*. The MIT Press

Varela, F. J. (1996). Neurophenomenology: A Methodological Remedy for the Hard Problem. In J. Shear (Ed.), *Explaining Consciousness: The Hard Problem* (1995th-7 by the Journal of Consciousness Studies ed., p. 337).

Varela, F. J., & Shear, J. (1999). First-person methodologies: What, why, how. *Journal of Consciousness Studies*, 6(2–3), 1–14.

Vicente, R., Wibral, M., Lindner, M., & Pipa, G. (2011). Transfer entropy—A model-free measure of effective connectivity for the neurosciences. *Journal of Computational Neuroscience*, 30(1), 45–67. <https://doi.org/10.1007/s10827-010-0262-3>

Wallis, J. D. (2007). Orbitofrontal Cortex and Its Contribution to Decision-Making. *Annual Review of Neuroscience*, 30(Volume 30, 2007), 31–56. <https://doi.org/10.1146/annurev.neuro.30.051606.094334>

Walter, N., & Hinterberger, T. (2022). Determining states of consciousness in the electroencephalogram based on spectral, complexity, and criticality features. *Neuroscience of Consciousness*, 2022(1), niac008. <https://doi.org/10.1093/nc/niac008>

Wilson, R. C., Takahashi, Y. K., Schoenbaum, G., & Niv, Y. (2014). Orbitofrontal cortex as a cognitive map of task space. *Neuron*, 81(2), 267–279. <https://doi.org/10.1016/j.neuron.2013.11.005>

Windt, J. M. (2015). Just in Time—Dreamless Sleep Experience as Pure Subjective Temporality. In T. Metzinger & J. M. Windt (Eds.), *Open MIND*. Open MIND. Frankfurt am Main: MIND Group. <https://doi.org/10.15502/9783958571174>

Zalesky, A., Fornito, A., & Bullmore, E. T. (2010). Network-based statistic: Identifying differences in brain networks. *NeuroImage*, 53(4), 1197–1207. <https://doi.org/10.1016/j.neuroimage.2010.06.041>

Zhang, X. S., Roy, R. J., & Jensen, E. W. (2001). EEG complexity as a measure of depth of anesthesia for patients. *IEEE Transactions on Bio-Medical Engineering*, 48(12), 1424–1433. <https://doi.org/10.1109/10.966601>

Ziv, J. (1978). Coding theorems for individual sequences. *IEEE Transactions on Information Theory*, 24(4), 405–412. IEEE Transactions on Information Theory. <https://doi.org/10.1109/TIT.1978.1055911>

Supplementary Materials

Supplementary Figure 1.

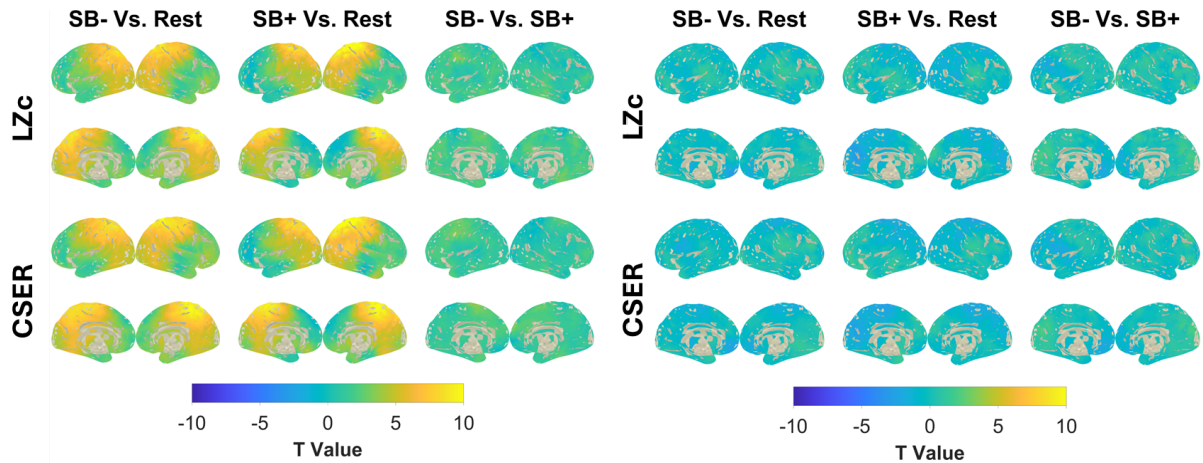


Figure S1. Left panel: Inflated cortical surfaces showing source level whole-group condition differences for broadband LZc and CSER showing all T-values, including insignificant voxels. **Right panel:** Inflated cortical surfaces showing source level differences between the subgroups of full dissolvers and others for broadband LZc and CSER showing all T-values, including insignificant voxels. For each condition pair, the difference in entropy rate values was taken and compared in a between-subjects design. Positive T values indicate higher neural difference values in the full dissolvers group.

Supplementary Figure 2.

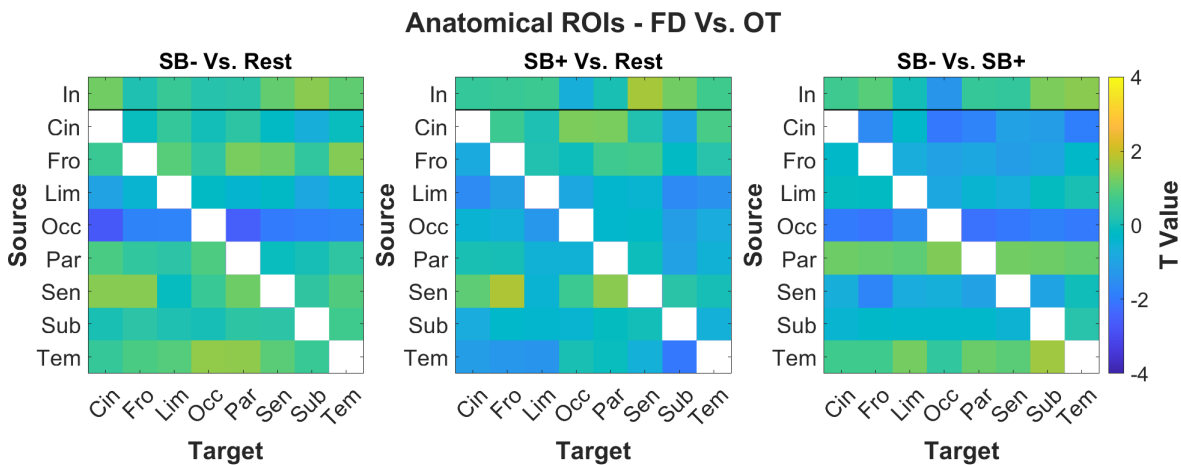
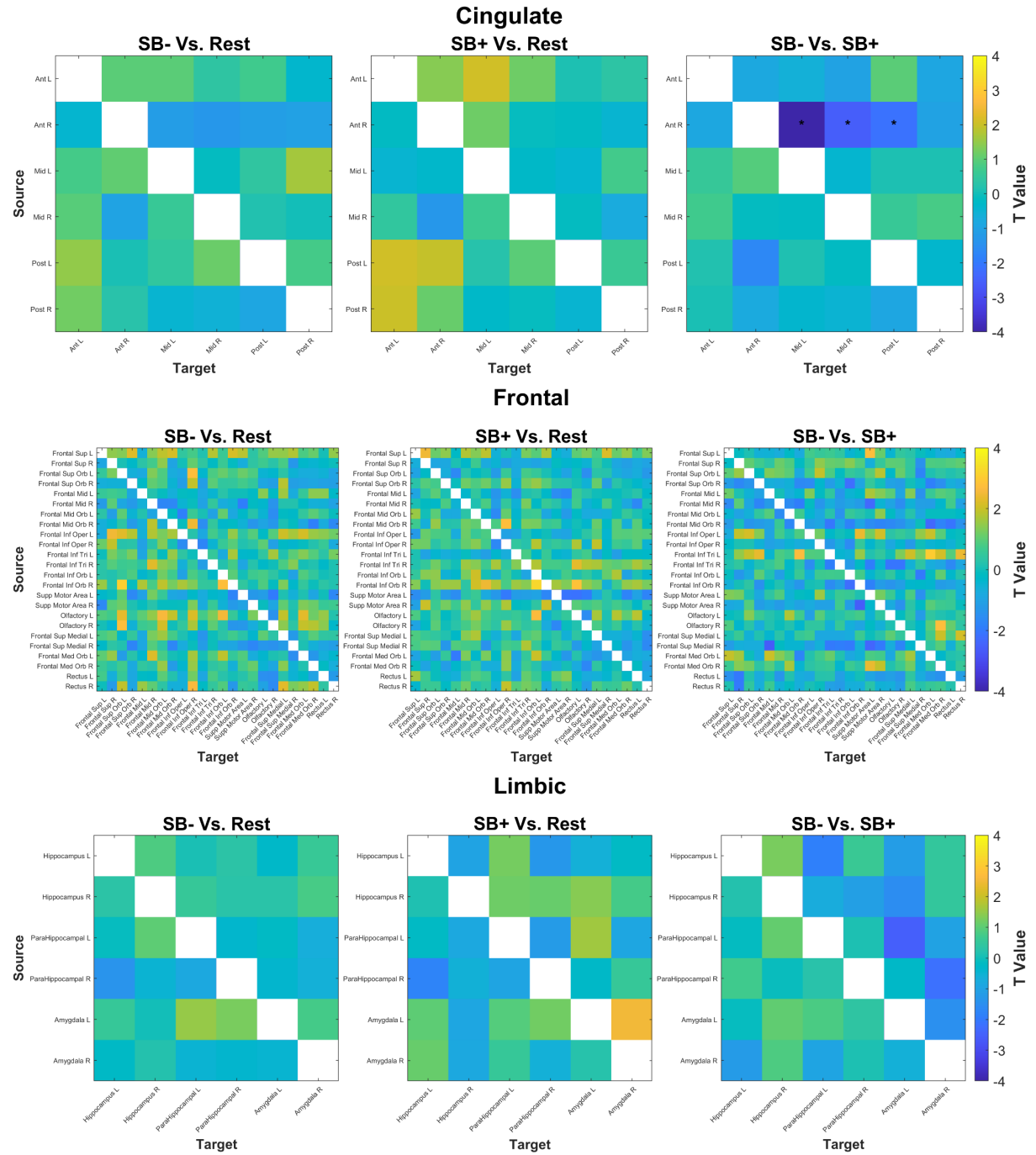
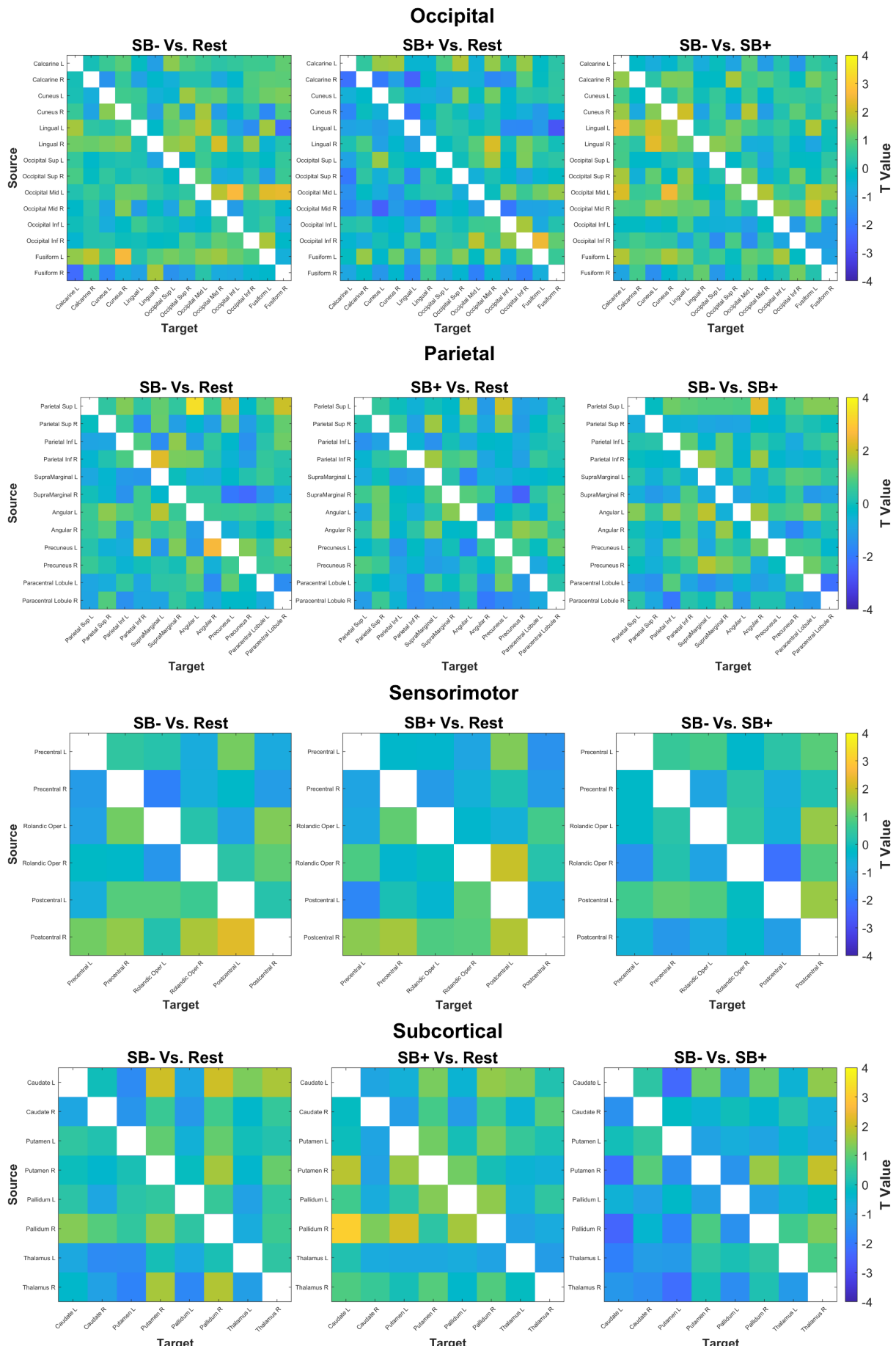


Figure S2. Heatmaps of Transfer Entropy within and between anatomical ROIs, for the full dissolvers vs. others comparison (denoted FD Vs. OT). Top row of each plot labeled “In” corresponds to global-conditional TE within each ROI. For each condition pair, the difference in TE values was taken and compared in a between-subjects design. Positive T values indicate higher neural difference values in the full dissolvers group. ROI abbreviations: Cin - Cingulate, Fro - frontal, Lim - limbic, Occ - occipital, Par - parietal, Sen - sensorimotor, Sub - subcortical, Tem - temporal.

Supplementary Figure 3.





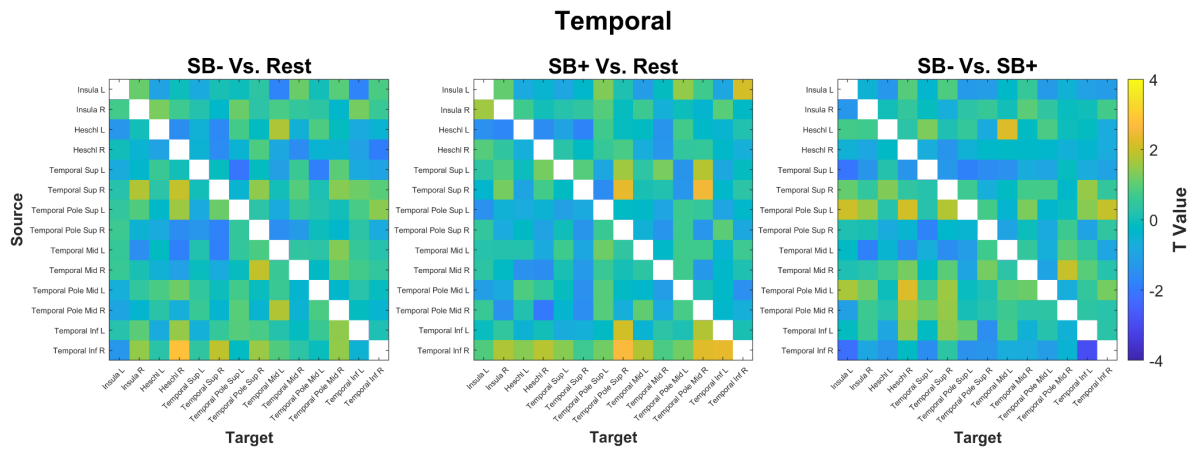
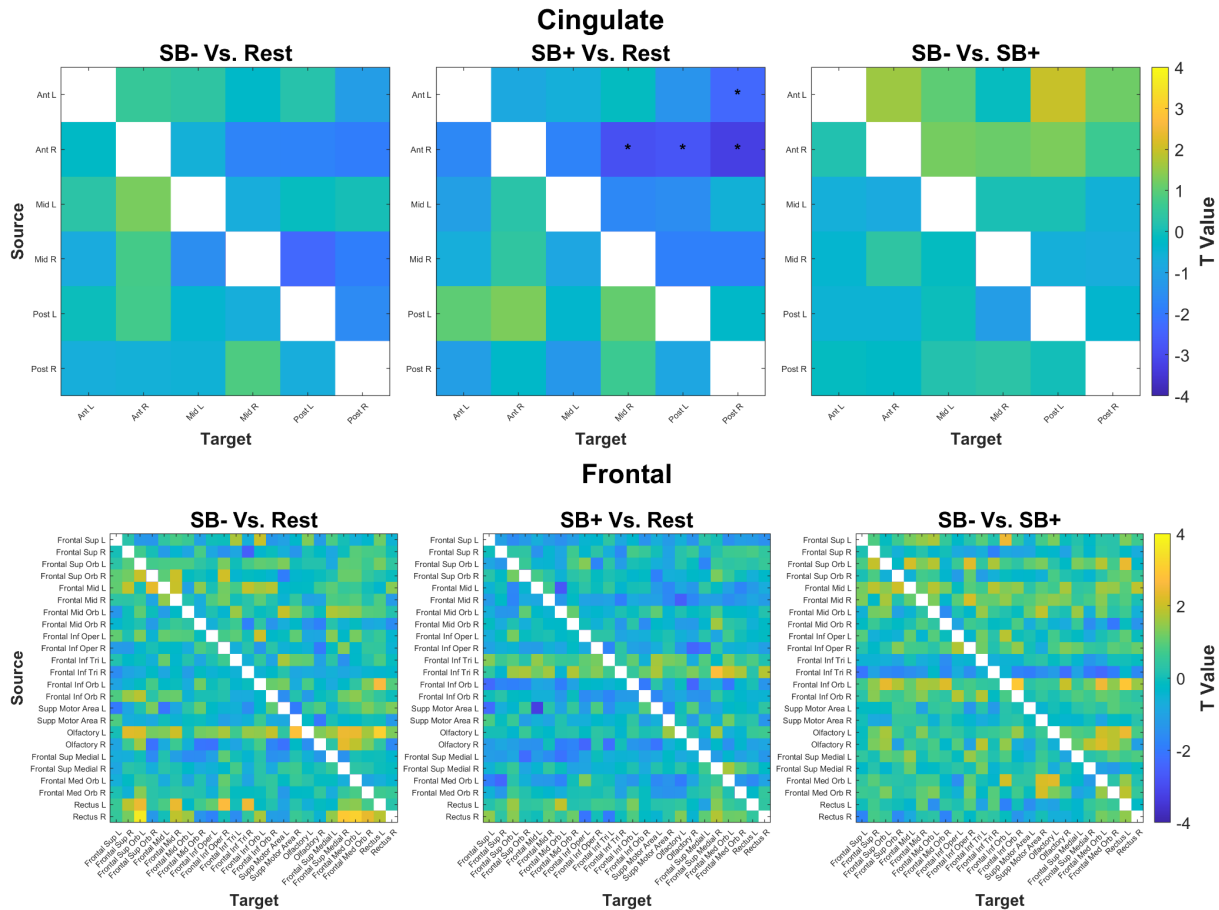
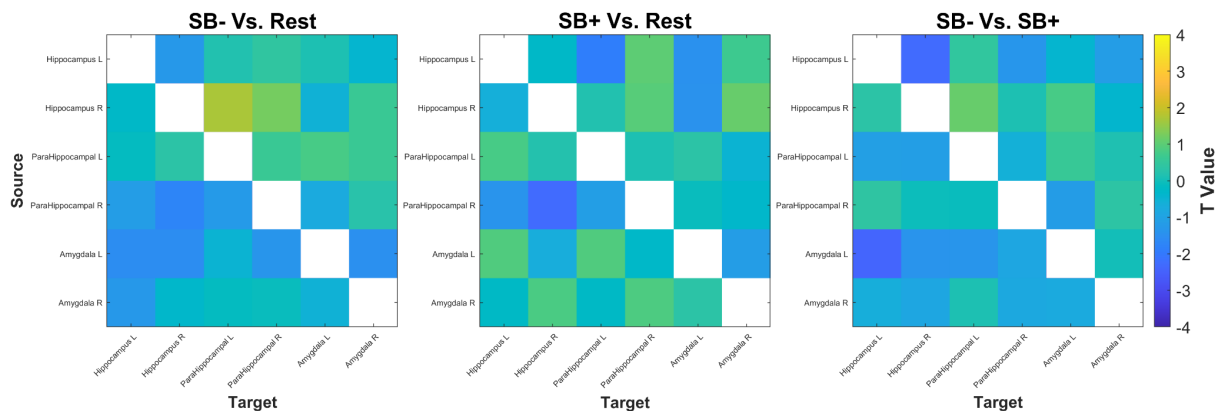


Figure S3. Heatmaps of *pairwise-conditional* Transfer Entropy within ROIs for the whole group comparison. Significant sub-networks identified through NBS at $p < 0.05$ are marked with an asterisk.

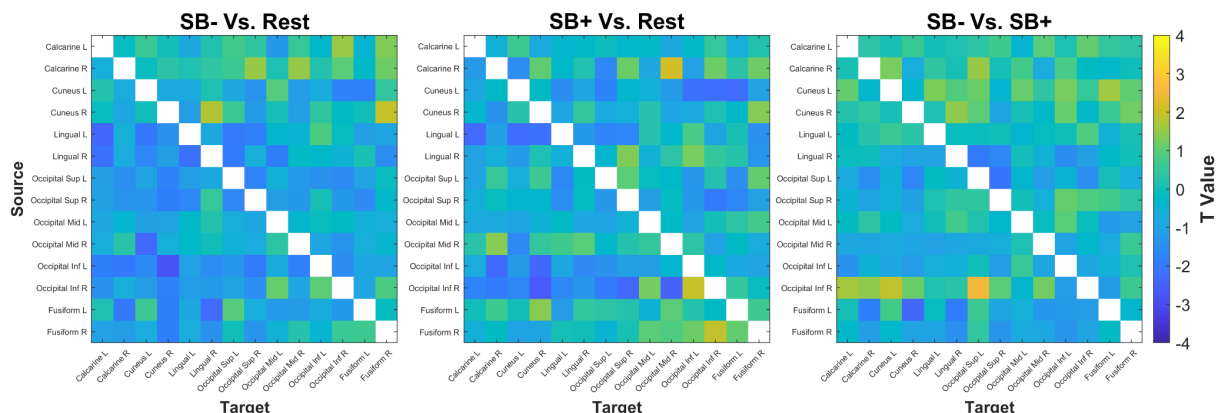
Supplementary Figure 4.



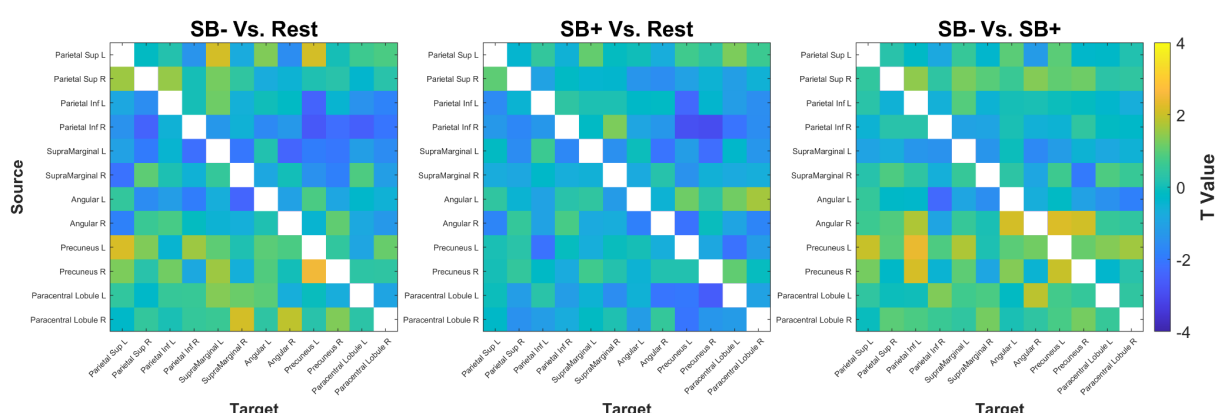
Limbic



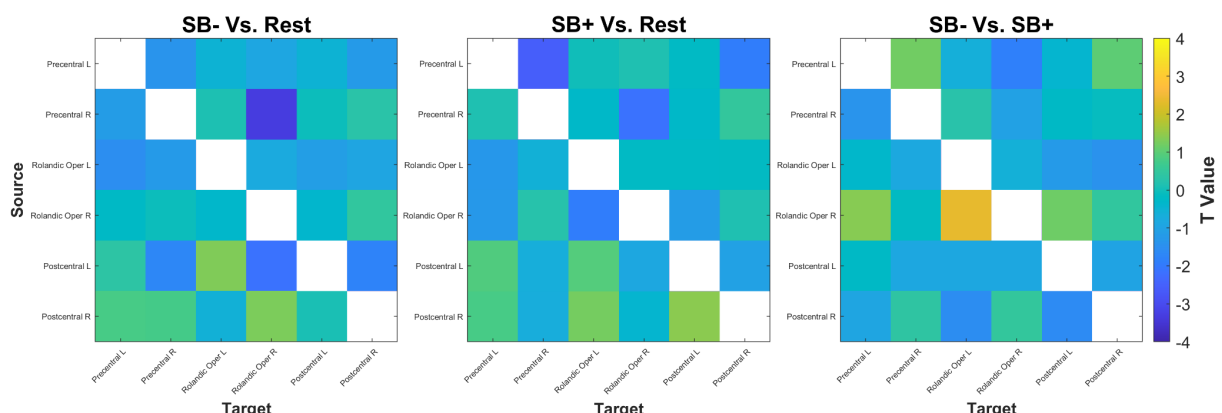
Occipital

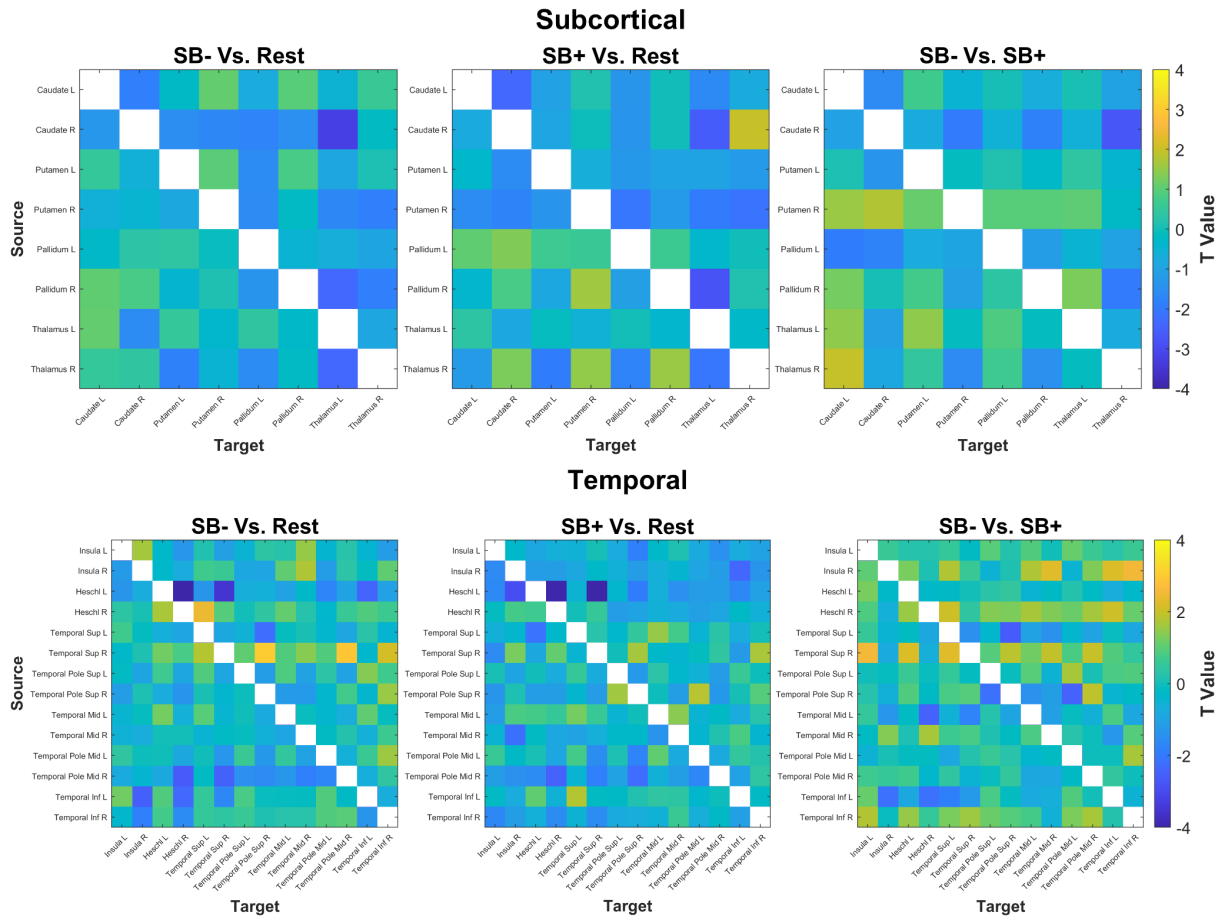


Parietal



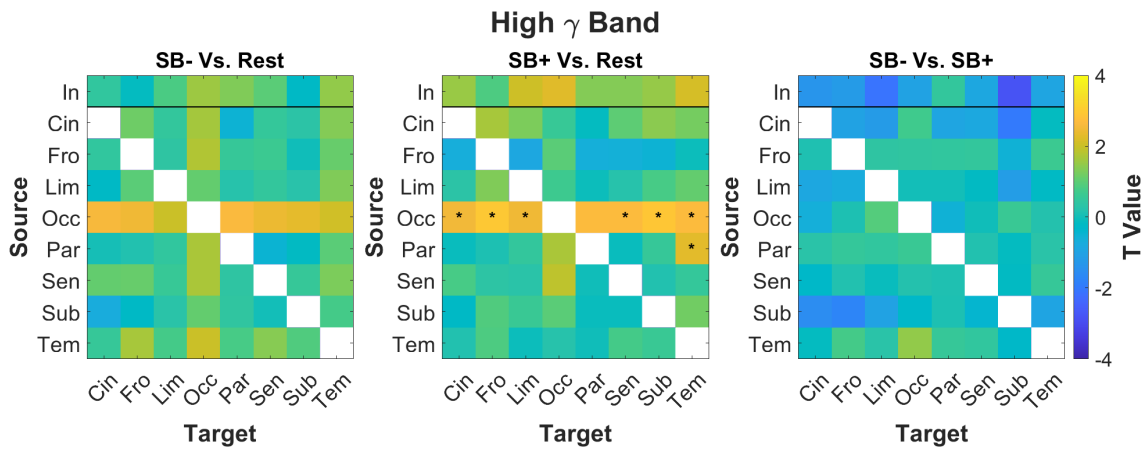
Sensorimotor

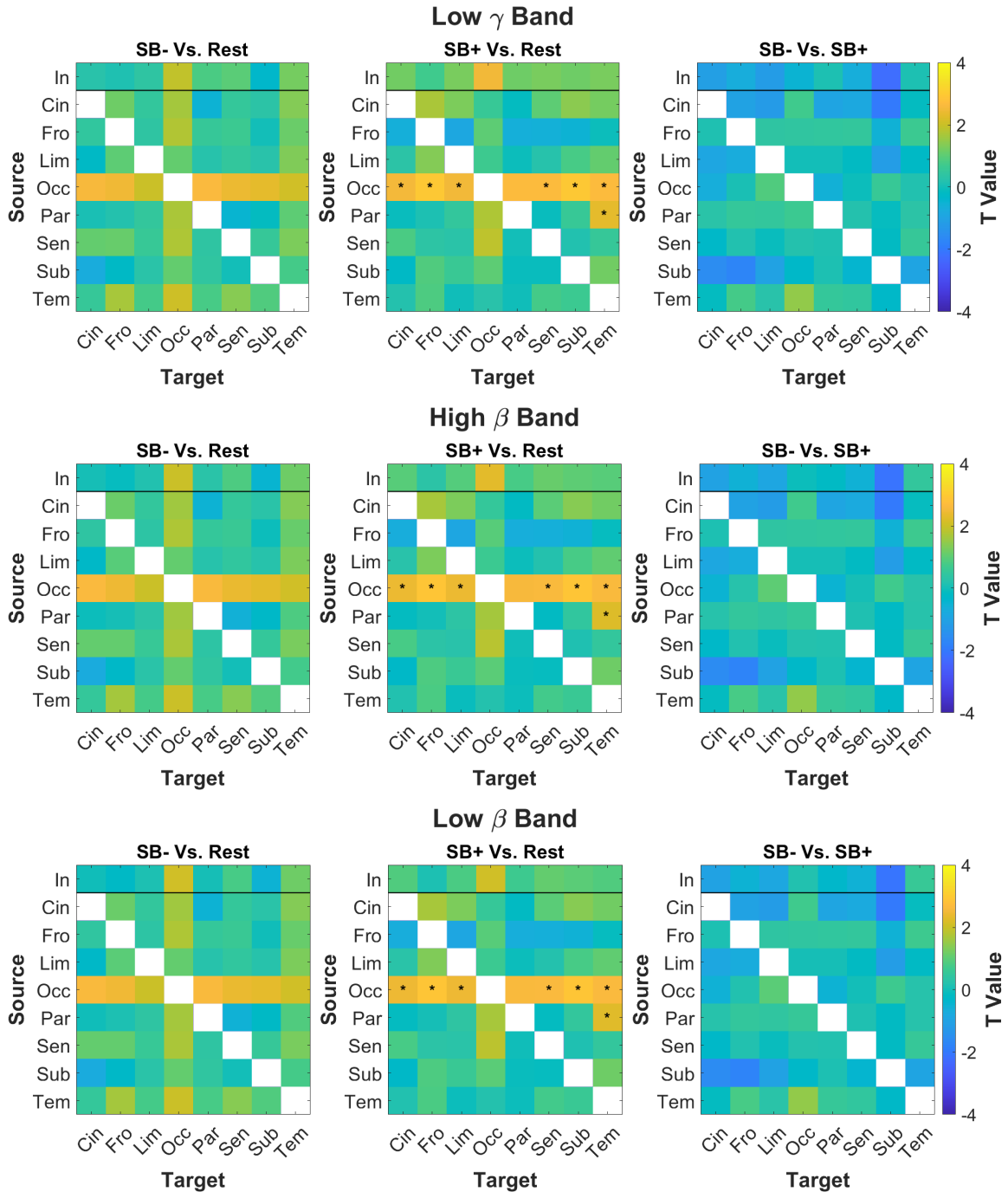


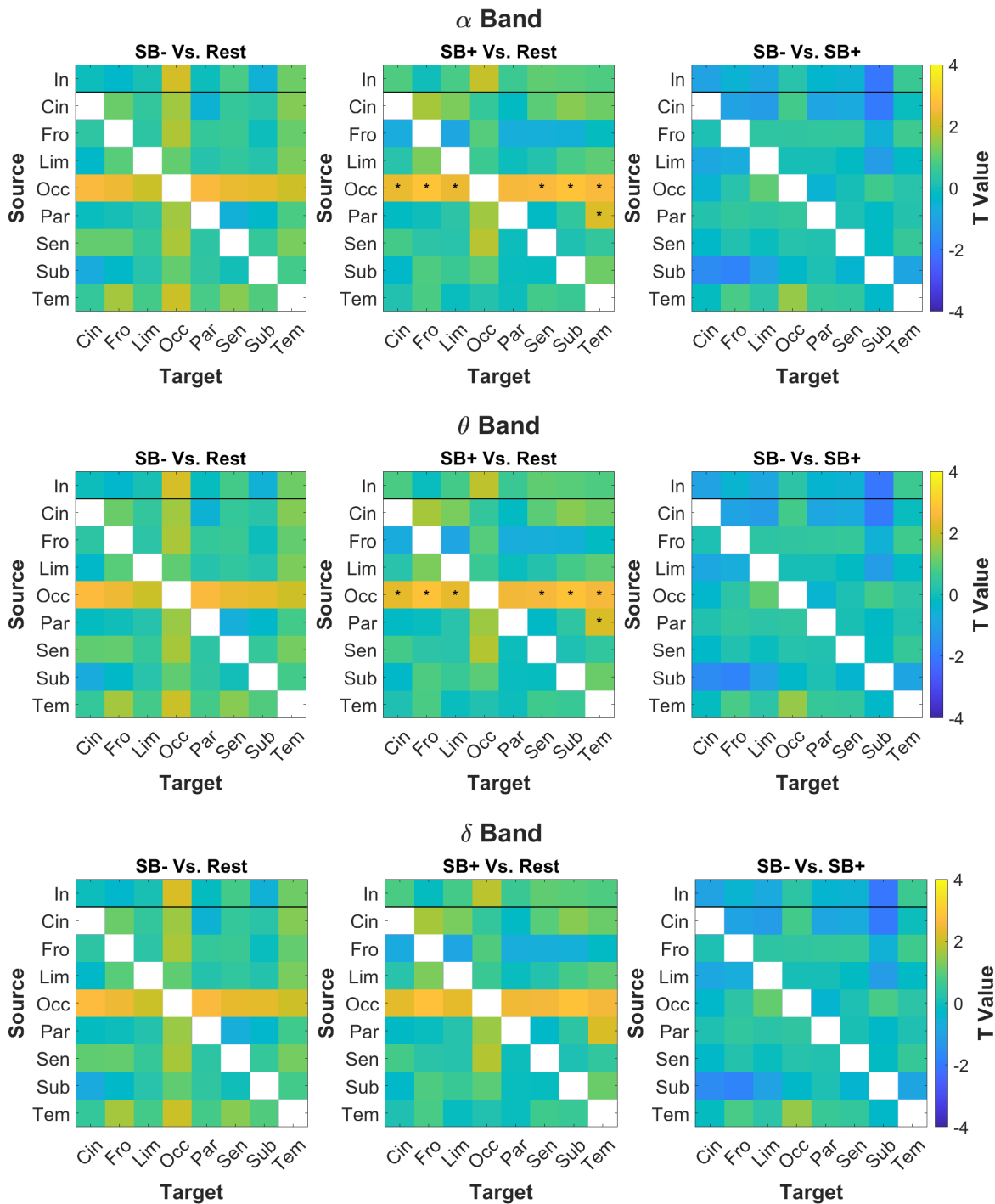


Supplementary Figure 4. Heatmaps of *pairwise-conditional* Transfer Entropy within ROIs for the full dissolvers vs. others comparison . Significant sub-networks identified through NBS at $p<0.05$ are marked with an asterisk. For each condition pair, the difference in TE values was taken and compared in a between-subjects design. Positive T values indicate higher neural difference values in the full dissolvers group.

Supplementary Figure 5.







Supplementary Tables

Band Name	Frequency Range
Delta	1-4 Hz
Theta	4-8 Hz
Alpha	8-12 Hz
Low Beta	12-20 Hz
High Beta	20-30 Hz
Low Gamma	30-60 Hz
High Gamma	60-100 Hz

Supplementary Table 1. Definition of frequency bands used for spectral decomposition of TE and CSER

ROI	AAL-116 Sources
Cingulate	Cingulum_Ant; Cingulum_Mid; Cingulum_Post
Frontal	Frontal_Sup; Frontal_Sup_Orb; Frontal_Mid; Frontal_Mid_Orb; Frontal_Inf_Oper; Frontal_Inf_Tri; Frontal_Inf_Orb; Supp_Motor_Area; Olfactory; Frontal_Sup_Medial; Frontal_Med_Orb; Rectus
Limbic	Hippocampus; ParaHippocampal; Amygdala
Occipital	Calcarine; Cuneus; Lingual; Occipital_Sup; Occipital_Mid; Occipital_Inf; Fusiform
Parietal	Parietal_Sup; Parietal_Inf; SupraMarginal; Angular; Precuneus; Paracentral_Lobule
Sensorimotor	Precentral; Rolandic_Oper; Postcentral
Subcortical	Caudate; Putamen; Pallidum; Thalamus
Temporal	Insula; Heschl; Temporal_Sup; Temporal_Pole_Sup; Temporal_Mid; Temporal_Pole_Mid; Temporal_Inf

Supplementary Table 2. Definition of anatomical regions of interest (ROIs) based on the AAL-116 atlas. Note that AAL sources are given here without the “left” or “right” labels, yet all refer to the AAL sources of both cortical hemispheres

Predictor	Estimate \pm SE	95% CI	p
Intercept	0.5049 \pm 0.0288	[0.4468, 0.5630]	<0.0001
β difference (X_{β})	-0.1025 \pm 0.0293	[-0.1617, -0.0434]	0.0011
LZc difference (X_{LZ})	-0.1185 \pm 0.0308	[-0.1807, -0.0562]	0.0004
TE difference (X_{TE})	-0.0919 \pm 0.0310	[-0.1545, -0.0294]	0.0050

Supplementary Table 3. Descriptive results of the multiple linear regression in section 3.3, using the three identified neural correlates (z-scored) as predictors of dissolution phenomenology score (see Fig. 7). Regression statistics: $R^2 = 0.5230$, adjusted $R^2 = 0.4872$, RMSE = 0.1929. X_{β} denotes SB-,SB+ difference in high-beta in the posterior-medial cortex, as calculated in Trautwein et al. (2024), X_{LZ} denotes SB-,SB+ difference in LZc in the orbitofrontal cortex, X_{TE} denotes SB-,SB+ difference in TE from cingulate, limbic, occipital and sub-cortical areas.